Double Networks: Hybrid Hydrogels with Clustered Silica

Anne-Charlotte Le Gulluche, Guylaine Ducouret, Ludovic Olanier, Annie Brûlet, Olivier Sanseau, Paul Sotta, Alba Marcellan

Double networks: hybrid hydrogels with clustered silica

Anne-Charlotte Le Gulluche,[†,‡] Guylaine Ducouret,[‡] Ludovic Olanier,[‡] Annie Brûlet,[¶] Olivier Sanseau,[§] Paul Sotta,[*,†,‖] and Alba Marcellan[*,‡,⊥]

†*Laboratoire Polymères et Matériaux Avancés, UMR5268, CNRS, Solvay, F-69192 Saint Fons cedex, France*

‡*Sciences et Ingénierie de la Matière Molle, UMR7615, ESPCI Paris, PSL University, Sorbonne Université, CNRS, F-75005 Paris, France*

¶*Laboratoire Léon Brillouin, UMR12, CEA, CNRS, Université Paris Saclay, C. E. Saclay, F-91191 Gif Sur Yvette cedex, France*

§*Solvay R&I PM2D, F-69192 Saint Fons Cedex, France*

‖*Ingénierie des Matériaux Polymères, UMR 5223, Université de Lyon, CNRS, Université Lyon 1, INSA Lyon, UJM, F-69621 Villeurbanne cedex, France*

⊥*Institut Universitaire de France*

E-mail: paul.sotta@insa-lyon.fr; alba.marcellan@espci.psl.eu

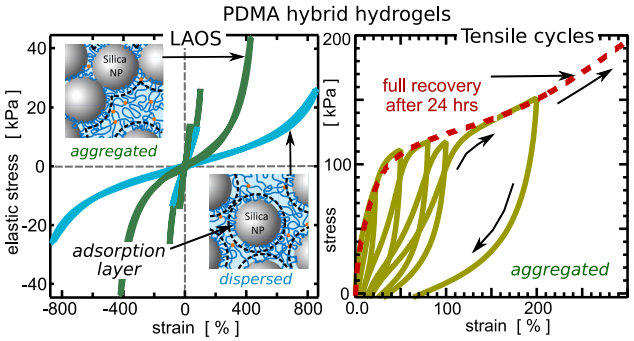

For Table of Contents use only

Abstract

Model hybrid hydrogels reinforced by silica nanoparticles were designed by polymerizing and cross-linking the gels in-situ. The polymer-particle interactions were tuned by using either poly(dimethylacrylamide) (PDMA), which adsorbs on silica, or poly(acrylamide) (PAAm), which does not. Besides, the dispersion state of silica nanoparticles was tuned from well-dispersed to aggregated by changing the pH from 9, which insures repulsive interactions between nanoparticles and good dispersion state, to about 6, which affects the surface chemistry of silica and promotes aggregation. The dispersion states were characterized by SAXS.

The mechanical behavior of hybrid gels with aggregated nanoparticles is markedly different from those where silica is well-dispersed within the matrix. PDMA-based hybrid gels display pronounced non-linear behavior, somehow similar to those observed in filled elastomers. The non-linearities are even more pronounced in gels with aggregated particles, with strong strain stiffening along with large dissipation. For those samples, reinforcement can be attributed to the combination of both reversible interactions between PDMA and silica nanoparticles, that provide strain-stiffening and recovery, and the response of the silica network. Recovery processes observed in hybrid gels with dispersed particles are preserved when silica particles are aggregated, but the characteristic time needed to fully recover the mechanical respnsee is extended from a few seconds to several hours.

In PAAm-based hybrid gels with aggregated silica nanoparticles, no recovery processes are observed. This implies that the properties, namely the very high linear tensile modulus and high dissipated energy, are driven by the rigid network formed by nanoparticle aggregation, that provides high dissipative capabilities, especially when compared to PAAm-based hybrid gels with dispersed silica, that remain soft and fragile. These gels exhibit a quite inhomogeneous structure with permanent damage under elongation.

The non-linear dynamical behavior of hybrid gels was investigated by Large Amplitude Oscillatory Shear (LAOS) experiments. While unfilled gels show no non-linearity

up to very large strain amplitude, marked non-linear effects combining a drop of modulus (similar to the Payne effect) and strain-stiffening for increasing strain amplitude, are observed in PDMA-based hybrid gels, certainly due to polymer adsorption onto nanoparticles. PAAm-based hybrid gels also show non-linearity, with a drop of modulus for increasing strain but no strain-stiffening, indicating that the presence of fillers alone can induce non-linearity in the absence of strong, reversible polymer-particle interactions. PAAm-based hybrid gels with aggregated silica show very high stiffness and high dissipative properties, at the expense of stretchability, though. Also, the structure seems to be permanently damaged under stress, revealing the importance of silica/polymer interactions for permanent mechanical reinforcement. Altogether, the analysis of the non-linear behavior indicates the importance of combining dynamic adsorption of polymer chains on silica nanoparticles with mechanical reinforcement provided by the silica network.

1 Introduction

Introducing solid nanoparticles in polymer matrices is a very efficient way to improve the mechanical properties of polymeric materials such as hydrogels[1–5] or elastomers.[6] Remarkably, both the elastic modulus and the elongation at break can be drastically increased, eventually leading to an enhancement of the energy at break or gel fracture toughness by several decades[6–11]. Besides, the materials may acquire self-repair and/or focussed repair capabilities.[2,3,12] Adhesion may also be tuned.[13]

In filled elastomers, it has been demonstrated that the reinforcement of mechanical properties is not simply a geometrical effect due to the presence of a solid fraction in the material, but is a consequence of the affected polymer dynamics at filler interfaces[14–18]. In hybrid gels, polymer adsorption is key for gel toughening, as shown by reported studies on PDMA/silica hybrid gels. Elucidating the various physical mechanisms at play and their relative contributions remains a key issue. Model systems have been elaborated and studied to solve this

question.[4,5] A primary objective has been to carefully control the structure of these model system, in terms of the distinct aspects of both the architecture of the network (controlled cross-link density and homogeneity of the network) and of the dispersion state of the reinforcing filler particles. Another objective has been then to carefully control the interactions between the polymer and the surfaces of the particles, while not affecting the other structural parameters of the materials.[4,5]

In a previous paper, the impact of polymer adsorption on mechanical properties and hydrogel toughening was assessed by tuning the reversible polymer/silica interactions.[19] This was achieved by various strategies. A first strategy was to change the nature of the monomer from N,N-dimethylacrylamide (DMA), which interacts with, that is, adsorbs on, silica through hydrogen-bonds,[20] to acrylamide (AAm), which does not,[21] while keeping constant other key parameters such as the surface chemistry and the dispersion state of the silica nanoparticles.

This difference in adsorption between DMA and AAm comes from a subtle balance of hydrogen bonds and hydrophobic contributions in both the monomer-silica and monomer-solvent interactions.[22]

The presence of an adsorbed polymer layer was evidenced by ^{1}H NMR relaxometry. This layer provides reversible cross-linking points within the PDMA network and dissipative mechanisms by network rearrangements. Since this feature was not observed in PAAm hybrid gels, the difference in the mechanical behavior of PAAm and PDMA hybrid gels was attributed to their respective ability to interact or not with silica nano-particles.

In a second strategy, the polymer/nanoparticle interactions were disturbed by tuning the surface chemistry of the nanoparticles. This was achieved by changing the pH of the solution.

Using SAXS experiments, it was confirmed that silica nanoparticles embedded in PDMA and in PAAm matrices were well-dispersed in both systems. The impact of reversible interactions alone could then be evaluated. Indeed, a specific challenge in hybrid hydrogels is to

tune polymer-particle interactions (or polymer adsorption) and the particle dispersion state in an independent way.

The concept of multiple networks has been developed following the work of Gong et al.[23–26] Interpenetrated networks are prepared by independent or successive crosslinking, with two different crosslink densities. Under large amplitude strain, the more densely crosslinked network shall break first, thus playing the role of a so-called sacrificial network, while the second network shall take over at large strain. In this way, a very efficient dissipative mechanism is introduced in the system, thus providing gels with drastically enhanced toughness. Note that movable crosslinks have also been proposed as a alternative dissipative mechanism.[27]

In this work, we want to check whether a similar double-network concept can be elaborated, with partially aggregated silica playing the role of the sacrificial network, so as to combine the high reinforcement potentially provided by solid nanoparticles at small or moderate strain, and the high dissipative efficiency and toughness provided by a sacrificial network at large strain. Our objective is also to discriminate two distinct dissipative mechanisms which may both potentially lead to enhancing the toughness of the hybrid gels. The first mechanism is the reversible chain adsorption on silica nanoparticles, which occurs when a PDMA gel matrix is used, in contrast to a PAAm matrix, in which polymer chains do not absorb on silica in aqueous solution. The second mechanism is the breaking of the reinforcing network formed by silica nanoparticles. This second mechanism is similar to what occurs in reinforced elastomers, in which the so-called Payne effect, that is the drop of the modulus at intermediate strain amplitudes, is generally attributed to the breakage of the filler network.[7,28–30] This breakage may be partially or fully reversible. One key question is thus the potential reversibility of these mechanisms.

In this context, the study presented in this paper has two objectives. First, besides the impact of the chemical nature of the monomer, the effect of the dispersion state of the silica on the mechanical properties will be assessed, by synthesizing hybrid gels with aggregated silica in PAAm and PDMA polymer matrices. Secondly, the non-linear behavior

will be explored more thoroughly using an experimental methodology developed for the study of filled rubbers in the first place[31], namely Large Amplitude Oscillatory Shear (LAOS) rheological measurements, performed on PDMA- and PAAm-based hybrid gels with either well-dispersed or aggregated silica nanoparticles.

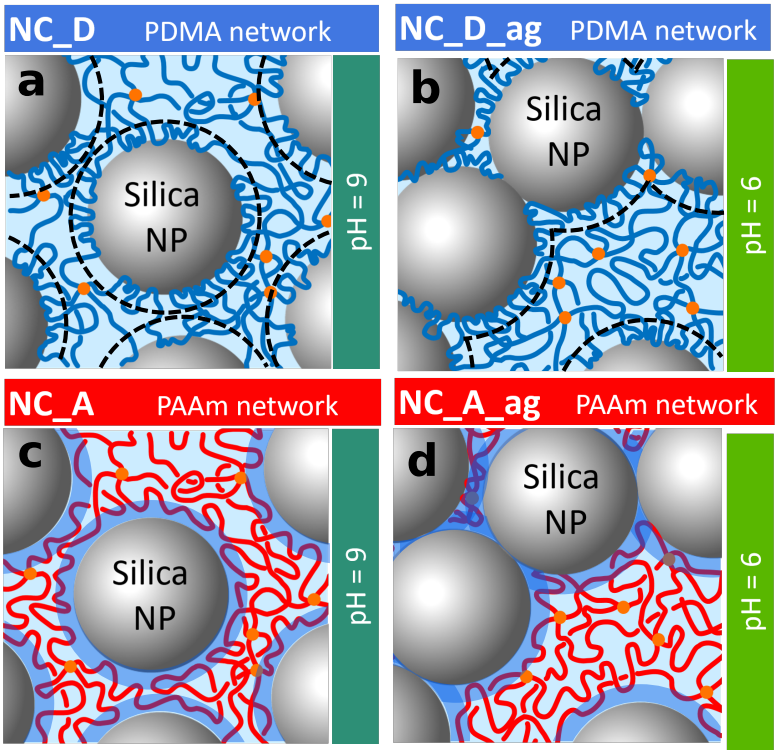

Figure 1: **a**: schematics of a PDMA hybrid hydrogel with dispersed silica nanoparticles (denoted NC_D) combining covalent cross-links (orange dots) and physical interactions (layer of adsorbed polymer chains at the surface of nanoparticles, schematized by dashed circles, not to scale); **b**: PDMA hybrid hydrogel with aggregated silica nanoparticles (NC_D_ag) forming a reinforcing network; **c**: PAAm hybrid hydrogel with dispersed silica nanoparticles (NC_A). Polymer chains do not adsorb on silica nanoparticles, eventually leading to a depletion layer (schematized in blue, not to scale); **d**: PAAm hybrid hydrogel with aggregated silica nanoparticles (NC_A_ag).

The general architecture of the studied hybrid hydrogels is schematized in Figure 1. The compositions of the hybrid gels were designed to obtain reproducible network topology and both high stretchability and stiffness. A small amount (0.1 mol%) of chemical cross-linker was used to control the network topology. This value enables obtaining a well-controlled cross-linking, overcoming the ill-controlled self cross-linking that may take place during poly-

merization,[2] and to maintain high extensibility. To enable quantitative comparison between samples, all materials were characterized in the gel preparation state, with a well-controlled gel matrix hydration and a fixed silica volume fraction $\varphi = 20$ vol%.

Dynamic oscillatory shear tests have been commonly used to investigate a wide range of soft matter and complex fluids with a recent renewal of interest in exploiting large amplitude oscillatory shear (LAOS) tests to investigate and quantify their complex nonlinear viscoelastic behavior[32–39]. Hybrid gels, which are composed of a dispersion of silica nanoparticles within a polymer matrix, present obvious similarities with filled elastomers. Submitted to large sinusoidal strains, filled elastomers were demonstrated to show a decrease in their storage modulus (Payne effect) along with nonlinear behavior (strain stiffening), meaning that their response is no longer purely sinusoidal[35,40].

The aim is to analyze more precisely the non-linearity of the mechanical response of the hybrid gels and to assess the similarities or differences with filled elastomers. Besides, the impact of the aggregation state of silica nanoparticles on the mechanical reinforcement and on the non-linear dynamical repsonse will be investigated.

The paper is organized as follows. The studied materials, synthesis procedure and experimental techniques are described in Section 2. The results are presented and discussed in Section 3. The way in which gels with aggregated particles are obtained is described in Section 3.1, the large scale structure of the silica reinforcing networks are described in Section 3.2, the mechanical properties in Section 3.4 and the non-linear properties measured in LAOS experiments are described in Section 3.5 for both well-dispersed and aggregated hybrid gels.

2 Materials and methods

2.1 Gel synthesis

Silica nanoparticles are Ludox-TM 50 produced by Grace and bought from Sigma-Aldrich in the form of a 50 wt% silica suspension in water at pH = 9. The nanoparticles were characterized by SEM and by Small Angle X-Ray Scattering. The particle diameter is 28 nm. SAXS curves were obtained in solutions diluted to 1 vol%. They were fitted with the form factor of polydisperse spherical particles with a Gaussian distribution of size, which gave a mean radius 13.5 nm with standard deviation $\sigma = 0.13$. The corresponding surface area is about 100 m^2/g, considering a silica density 2.3 g/cm^3.

Hydrogels were prepared at room temperature by *in situ* free radical polymerization using N, N'-methylenebisacrylamide (MBA) as cross-linker and KPS/TEMED as redox initiators.[19] Acrylamide (AAm, 99% electrophoresis grade, Aldrich), N, N-dimethylacrylamide (DMA, 99%, Aldrich), N, N'-methylenebis(acrylamide) (MBA, 99%, Aldrich) and N, N, N', N'-tetramethyl ethylenediamine (TEMED, 99% bio reagent, Aldrich), potassium persulfate (KPS, > 99%, ACS reagent, Aldrich) and (3-Aminopropyl)triethoxysilane (APTES, 99%, Aldrich) were used as received. All reactants were deoxygenated and introduced in a nitrogen-filled overpressured glove box ($O_2 < 5$ ppm) in order to prevent any oxygen contamination. Solid reagents were initially dissolved in water (KPS: 4,5 wt%, MBA: 1,5 wt%) prior to synthesis. After diluting the Ludox-TM50 silica suspension in de-ionized (DI) water, the pH was readjusted to 9 using either HCl or NaOH. Alternatively, in order to promote nanoparticle aggregation, the pH was changed to a range from 5 to 6 using HCl. The MBA solution and the monomer were then added in the suspension. The resulting solution was vigorously stirred and cooled down with ice-patches. Solutions of KPS and of pre-cooled (0°C) TEMED were added under stirring. The mixture was then rapidly transferred into home-made moulds placed in the glove box. The mould geometries were chosen depending on the subsequent characterization techniques. Redox initiation started rapidly (in agreement

with observations by Orakdogen[41]) and polymerization was left to proceed for 24 hours. After demolding, hydrogels were immediately characterized or stored in paraffin oil to avoid drying before analysis.

For all syntheses, the monomer/KPS and monomer/TEMED molar ratios were fixed at 100. The crosslinker/monomer (MBA/monomer) molar ratio was kept constant at 0.1 mol%. The silica volume fraction was fixed at 20 vol% for all hybrid hydrogels. Hydrogels were studied in the preparation state, with a fixed monomer/water molar ratio equal to 0.025.

The nomenclature used in this study is M for unfilled, crosslinked gels (unfilled matrices), NC for nanocomposite samples (hybrid hydrogels at 20 vol% silica nanoparticles), A for AAm-based and D for DMA-based gels. For instance, the unfilled PAAm gel (cross-linked at 0.1 mol%) is denoted MA and a PDMA gel cross-linked with a MBA molar ratio of 0.1 mol% and containing 20 vol% silica is denoted NC_D. Hydrogels with aggregated silica (synthesized at pH 6) are labeled with an additional _ag suffix. The hydrogel nomenclature and formulations are reported in Table 1.

Table 1: Compositions of hydrogels. For all compositions, the amounts of co-initiators were $m_{KPS} = 0.041$ g and $v_{TEMED} = 22.5$ μL, and the amount of chemical cross-linker was $m_{MBA} = 2.3$ mg. The silica volume fraction, defined as the ratio of the silica nanoparticle volume to the total volume of hybrid hydrogels, was fixed at 20 vol% for all hybrid compositions.

Sample	Nomenclature	m_{Si}/g	m_{water}/g	$m_{monomer}$/g
PDMA, unfilled	MD	0	10.621	1.487
PAAm, unfilled	MA	0	10.621	1.069
PDMA, dispersed	NC_D	7.063	10.621	1.487
PAAm, dispersed	NC_A	7.063	10.621	1.069
PDMA, aggregated	NC_D_ag	7.063	10.621	1.487
PAAm, aggregated	NC_A_ag	7.063	10.621	1.069

2.2 Equilibrium swelling measurements

The swelling behavior was investigated in DI water at pH 9 (hybrid gels with well-dispersed silica) or pH 6 (hybrid gels with aggregated silica). The as-prepared samples were weighed

and put in a large excess of solvent for 15 days. The volume swelling ratios in the initial (preparation) state Q_0 and at swelling equilibrium Q_e are computed as follows, assuming negligible extractible (sol) content and additivity of volumes:

$$Q_0 = 1 + \frac{\nu_w}{\nu_p}\left(\frac{m_g^0}{m_p^0} - 1\right) \tag{1}$$

$$Q_e = 1 + \frac{\nu_w}{\nu_p}\left(\frac{m_g^{(e)}}{m_p^0} - 1\right) \tag{2}$$

where v_{spe}^p is the specific volume of the dry polymer network ($v_p = 0.95$ mL/g for DMA and 0.709 mL/g for AAm), v_w is the specific volume of the solvent (1 mL/g for water), m_g^0 is the mass of the gel in the initial (preparation) state, $m_g^{(e)}$ the mass of the gel at equilibrium swelling and m_p^0 the mass of the dry polymer network. The swelling ratio refered to the preparation state is then defined as $S_R = Q_e/Q_0$.

2.3 Mechanical tests

Gel samples used for mechanical tests were synthesized in home-made moulds consisting of two covered glass plates spaced by a 2 mm thick stainless steel spacer. The gels were then cut with a puncher into specimens of length $L_0 = 25$ mm, width $w_0 = 5$ mm and thickness $t_0 = 2$ mm.

Tensile tests were performed on a standard Instron model 5565 tensile device, using a 10 N load cell (relative uncertainty 0.16% in the range 0 to 0.1 N) and a SVE video extensometer (relative uncertainty 0.11% at full scale). Gel samples were placed in home-made screw side-action grips. To avoid any drift in the gel composition during experiments or after 24h recovery, gels were immersed in paraffin oil. The strain is defined throughout as the nominal (or Cauchy) strain $\epsilon_N = \Delta L/L_0$, with $\Delta L = L - L_0$ where L and L_0 are respectively the stretched and initial lengths, as obtained from the optical extensometer. The nominal (or engineering) stress σ_N was calculated from the tensile force F as $\sigma_N = F/(w_0 t_0)$, where $w_0 t_0$

is the initial cross section area (5×2 mm^2). The true stress σ_T was calculated assuming iso-volume deformation $\sigma_T = \lambda\sigma_N$ where $\lambda = L/L_0 = 1 + \epsilon_N$ is the draw ratio. The nominal strain rate was maintained constant at 0.06 s^{-1}. Tensile moduli were estimated by taking the initial slopes of the curves (typically between 0 and 1% strain for aggregated systems and between 0 and 10% strain for dispersed systems).

Loading-unloading cycles were performed in order to investigate self-recovery of the gels and the characteristic times of viscoelastic mechanisms. Cycles at constant strain rate were applied from 0 to a maximum strain ϵ_0 and then the sample was unloaded.

2.4 Rheological measurements

A stress-controlled DHR-3 rheometer from TA Instruments equipped with a stainless steel plate/plate geometry (diameter 20 mm) was used. A schematic of the cell specifically designed to mould hybrid gel samples for ocillatory shear experiments is shown in Figure 2. The home-made mould is made of two glass disks (22 mm diameter) separated by a 2 mm thick removable stainless steel spacer. To prevent slippage and surface effects,[42] gels were covalently grafted to the glass disks using (3-aminopropyl)triethoxysilane (APTES) as coupling agent. Prior to grafting, the glass plates were cleaned using a cerium oxide suspension (20wt% in water) and RBS detergent (10wt% in water). After drying, they were treated with a solution of APTES at 2wt% in absolute ethanol in the presence of hydrochloric acid, then heated to 100 °C in an oven for 10 minutes. The glass plates were then glued on a disposable plate-plate geometry, using a bi-component epoxy glue as depicted in Figure 2. Drying of the samples was prevented by immersing them into paraffin oil during measurements.

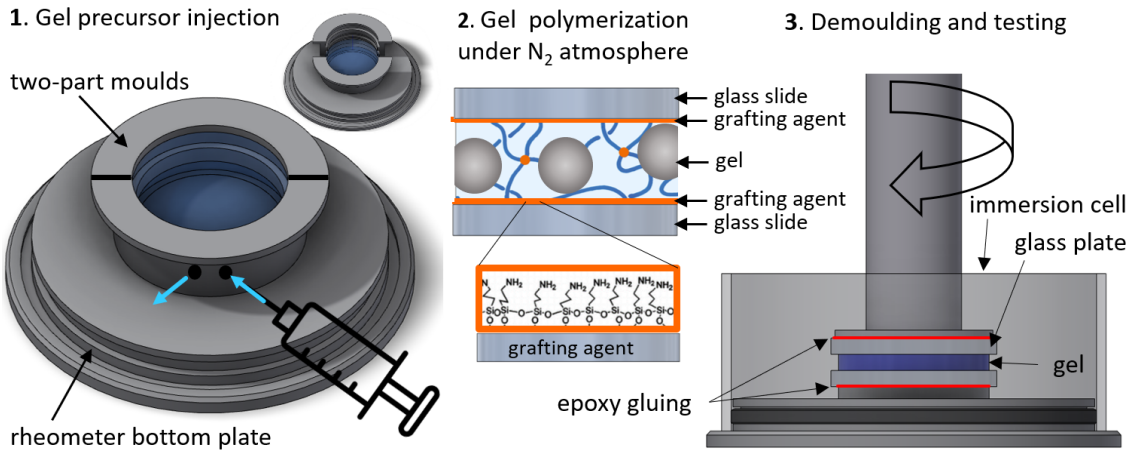

Figure 2: Schematics of the procedure developed for gel sample preparation and LAOS measurements. Samples are injected in between covalently grafted glass plates and left to polymerize until gelation. Glass plates are then glued onto the disposable rheology cell.

Frequency sweeps from 1 to 100 rad.s^{-1} were performed in the linear viscoelastic plateau at 0.1% strain amplitude (measured at the outer diameter of the cell). Large Amplitude Oscillation Shear (LAOS) strain was applied at a fixed frequency of 1 Hz. The strain amplitude was varied from 0.1 % to various maximum values depending on the considered hydrogel (800% for NC_D, 150 % for MD_R01 and MA_R01, 250 % for NC_A, 450 % for NC_D_ag and NC_A_ag).

Analyzing large Amplitude Oscillation Shear

The time-dependent torque and angular displacement signals were recorded with 1000 points per period. For each strain amplitude, the strain was applied during 30 s (30 oscillation periods) and the acquisition was made on the last 20 s to get rid of the transient regime. In plate-plate rotational geometry, the shear is not uniform, which is a downside for non-linear measurements. Assuming that the response is dominated by the outer ring of the disk-shaped sample, the stress σ (in Pa) and strain γ were calculated from raw data as $\sigma = 2T_m/(\pi R^3)$, where T_m is the measured torque (in N.m) and R is the radius of the cell (in m), and $\gamma = R\theta/w_s$, where θ is the angular displacement (in rad) and w_s the sample thickness (in m) (see the Supplementary Information (**SI**) file).

In the linear viscoelastic regime, the stress response to a sinusoidal strain is purely sinu-

soidal, with components in phase with $\gamma(t)$ (elastic response) and in phase with $\dot{\gamma}(t)$ (viscous response), from which the storage $G'(\omega)$ and loss $G''(\omega)$ moduli are obtained, respectively[43]. In the non-linear regime, the stress response may not be sinusoidal any longer. Several approaches have been proposed to describe the observed non-linear behavior[44–47]. In the method proposed by Cho et al.[48], under a large amplitude oscillatory strain of the form $\gamma = \gamma_0 \sin(\omega t)$ (which is an odd function of time t), the non-linear (but still periodic) stress $\sigma(t)$ is decomposed into the sum of an odd ($\sigma'(t)$, in phase with $\gamma(t)$, elastic) and even ($\sigma''(t)$, in phase with $\dot{\gamma}(t) = \gamma_0 \omega \cos(\omega t)$) components according to:

$$\sigma(t) = \sigma'(t) + \sigma''(t) \tag{3}$$

with

$$\sigma'(t) = (\sigma(t) - \sigma(-t))/2 \tag{4}$$

$$\sigma''(t) = (\sigma(t) + \sigma(-t))/2 \tag{5}$$

The generalized moduli Γ' and Γ'' are then defined as:

$$\sigma'(t) = \Gamma' \gamma(t) \tag{6}$$

$$\sigma''(t) = \Gamma'' \dot{\gamma}(t)/\omega \tag{7}$$

In the linear regime, generalized moduli coincide with G' and G'' respectively. In the non linear case, the moduli Γ' and Γ'' may depend on the values of γ(t) and $\dot{\gamma}$(t) within each strain cycle, meaning that the plots of σ' versus γ and of σ'' versus $\dot{\gamma}/\omega$ may deviate from straight lines. This method enables analyzing the non-linear viscoelastic behavior of a sample inside each cycle. It was used for studying viscoelastic soft materials such as organogels[49], fibrin gels and other hydrogels[36–38,50,51], amphiphilic polymer solutions[52], PDMS[53] and filled elastomers[35,40]. Note that the 3D so-called Lissajous-Bowditch representation may be used

to visualize the elastic and viscous stress contributions defined in equations 4 and 5 in a single combined graph.[39]

2.5 Small Angle X-Ray Scattering

Samples were prepared according to the synthesis protocole described in Section 2.1 and directly injected in poly(imide) capillar tubes (MicroLumen) of diameter 1.5 mm under nitrogen atmosphere, which were then welded to prevent drying. For calibration and comparison, solutions of silica nanoparticles were also prepared with volume fractions varying from 0.18 to 0.33 (pure Ludox suspension). SAXS experiments were carried out at Laboratoire Léon Brillouin (CEA, Saclay) with a Xeuss 2.0 instrument from Xenoxs (Grenoble, France) equipped with a PILATUS3 1M detector of dimension 168.7×179.4 mm. The range of scattering vector q was 0.0038 to 0.1 $Å^{-1}$. Absolute intensities $I(q)$ (in cm^{-1}), obtained after subtraction of empty capillary and electronic background and normalization by the sample transmission and thickness, were analyzed using the SASView v3.2.1 software.

3 Results and discussion

First, the impact of lowering the pH on the silica dispersion state of PAAm and PDMA hybrid gels will be assessed. Then the swelling behavior and the mechanical properties of hybrid gels synthesized at pH = 9 or at acid pH (pH = 6) will be investigated, with a special emphasis on the non linear behavior. The non linear behavior is then further analyzed with Large Amplitude Oscillatory Strain (LAOS) experiments.

3.1 Aggregating silica in hybrid gels networks

The surface chemistry of silica drives its ability to promote polymer adsorption as well as to remain stable in aqueous suspension[54]. It is here purposely tuned to promote aggregation of the nanoparticles within the network. Lowering the pH in the range 5 to 6 increases the

density of silanol groups and reduces the density of silanolates at the silica surface, thus decreasing electrostatic repulsions between particles that ensure the suspension stability. However, increasing the silanol surface density also increases the strength of PDMA and PAAm interactions with silica[55,56], and this effect may act against aggregation to some extent.

Preliminary experiments conducted on Ludox TM-50 silica suspensions indeed show that lowering the pH favors aggregation of silica nanoparticles within a few days at room temperature. On the other hand, at pH = 6, gelation of hybrid gels, specifically PAAm hybrid gels (NC_A_ag), proceeds within seconds after adding the KPS and TEMED initiators. Several ways were explored to delay gelation. For PDMA gels (NC_D_ag), thermal initiation of KPS at 80°C gave good results. Conversely, for PAAm gels (NC_A_ag), only weak silica aggregation was observed, as the samples remained soft and transparent even at pH = 6. Redox initiation was prefered, though it requires strict control of temperature and stirring. Keeping good control of aggregation turned out to be very difficult and relatively large disparities between samples were obtained. The syntheses performed at pH = 6 yielded turbid and stiff gels, indicating that the silica dispersion state was indeed drastically affected by the pH.

3.2 SAXS structural characterization of hybrid gels

Scattering curves of the samples synthesized at pH = 9 (NC_D and NC_A) and at pH = 6 (NC_D_ag, NC_A_ag) are shown in Figure 3. The scattering patterns of all hybrid gels (which all have the same particle volume fraction 20 vol%) superpose in the high q range ($q \geq 2.4$ Å^{-1} typically), as they are determined by the form factor of individual particles and a constant number of particle per unit volume. However, in the low-q regime, the curves for aggregated samples (NC_A_ag and NC_D_ag) significantly differ from those for dispersed ones, with a large increase in intensity at low q, related to aggregation, and the disappearance of the correlation peak present in the curves of NC_D ($q_{max} = 0.0188$ Å^{-1}) and NC_A ($q_{max} = 0.0168$ Å^{-1}). This peak corresponds to repulsive interactions with an

average near-neighbor distance of order $2\pi/q_{max} = 33 - 34$ nm, a little larger than the particle diameter. For NC_A_ag and NC_D_ag, the potential between particles becomes clearly attractive and aggregation is promoted.

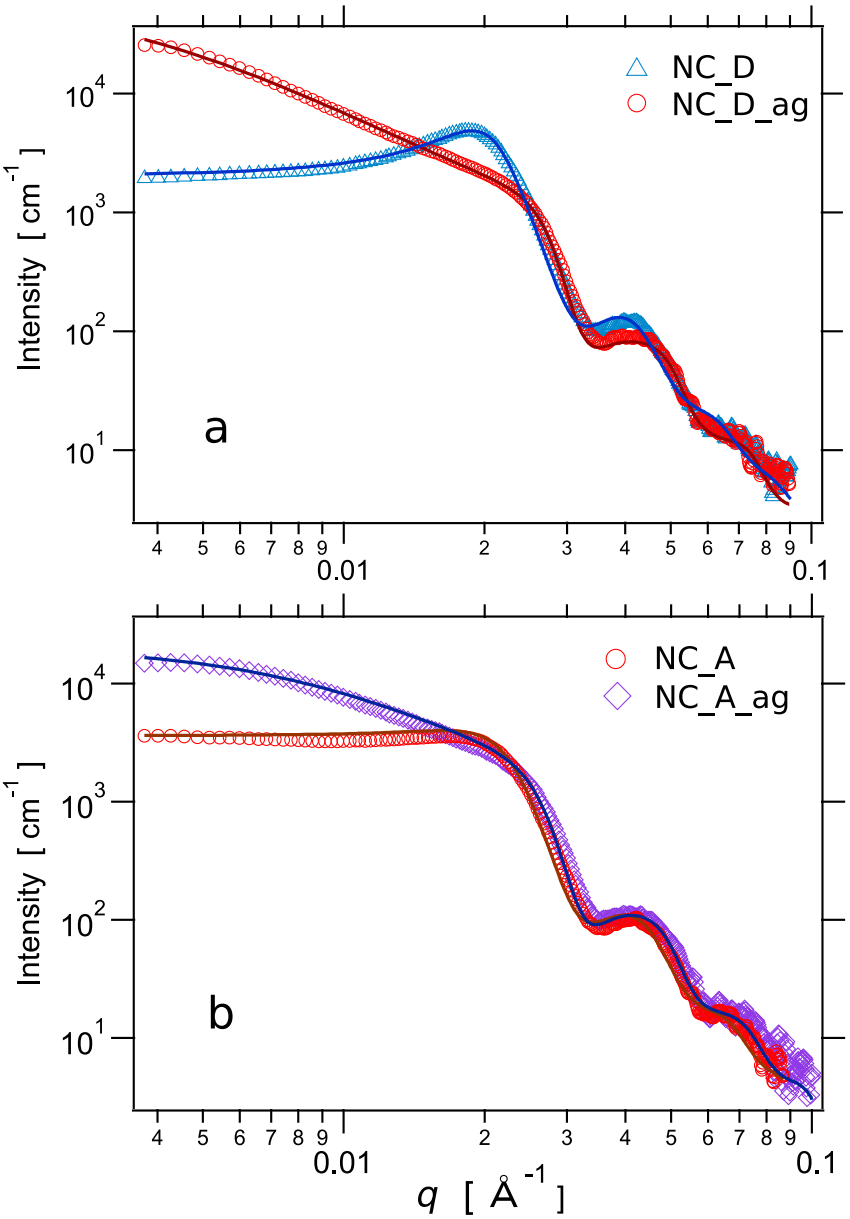

Figure 3: **a.** Scattering intensities of: **a**: NC_D and NC_D_ag samples; **b**: NC_A and NC_A_ag samples. The plain curves are the corresponding fits based on the Sticky Hard Sphere model. The silica volume fraction is with $\varphi_{Si} = 0.2$ for all samples.

The curves were fitted using a hard sphere form factor with a Gaussian distribution of radii and an interparticle structure factor $S(q)$ calculated for a hard sphere fluid with a

narrow attractive well, using a perturbative solution of the Percus-Yevick closure (sticky hard sphere model)[57,58]. The interaction potential $U(r)$ is defined as :

$$U(r) = \begin{cases} \infty, r < \sigma_{int} \\ U_0, \sigma_{int} \leq r \leq \sigma_{int} + \Delta \\ 0, r \geq \sigma_{int} + \Delta \end{cases} \tag{8}$$

with Δ, the width and U_0 the depth (in k_BT units) of the square well and $\sigma_{int} = 2r_{Si}$ the hard sphere diameter. The stickiness τ_{int} is defined as:

$$\tau_{int} = \frac{1}{12\epsilon_p} \exp(U_0) \tag{9}$$

with $\epsilon_p = \Delta/(\sigma_{int} + \Delta)$ the so-called perturbation factor. U_0 is negative (resp. positive) for an attractive (resp. repulsive) potential. Smaller values of τ_{int} correspond to stronger attraction.

The fitting curves obtained with the Sticky Hard Sphere model are shown in Figure 3. The quality of the obtained fits shows that there is no need to introduce long range electrostatic repulsions between particles in the fitting function. This indicates that hard sphere repulsions and short-range attractions are predominent, as the systems are quite concentrated (volume fraction 20%). Fitted parameter values are summarized in Table 2. Adjusted parameters are the perturbation factor ϵ_p and stickiness factor τ_{int}. The particle radius $r_{Si} = 13.4$ nm was obtained by fitting the scattering curves of silica suspensions. Volume fractions are determined by the synthesis.

Table 2: Fitted parameters of the sticky hard sphere interaction potential obtained for the dispersed (NC_D, NC_A) and aggregated (NC_A_ag and NC_D_ag) hybrid gels.

Parameter	NC_D	NC_A	NC_D_ag	NC_A_ag
Volume fraction	0.23	0.22	0.23	0.22
ϵ_p	0.1 ± 0.001	0.095 ± 0.01	0.090 ± 4.10^{-12}	0.03 ± 0.006
τ_{int}	5680 ± 0.06	2.1 ± 0.08	0.011 ± 0.0003	0.164 ± 0.0007
U_0/k_BT	8.83	0.873	-4.43	-2.83
interaction	repulsion	repulsion	strong attraction	moderate attraction

The stickiness factor is higher in NC_D than in the corresponding NC_A sample, which confirms that PAAm has a tendency to promote aggregation as it does not adsorb on silica. Nevertheless, silica particles remain well dispersed in both NC_A and ND_D hybrid gels. For hybrid gels synthesized at lower pH, the fitted τ_{int} values are considerably smaller, corresponding to negative values of U_0, which indicates strong aggregation. Particles seem to be a little less aggregated in NC_A_ag than in NC_D_ag, though.

In between roughly $q \approx 0.008$ and $q \approx 0.02$, a regime with an apparent power law $I \sim q^{-1.5}$ is observed in both aggregated systems. This suggests that particles tend to form disordered chain-like aggregates.[59,60] In the context of polymer nanocomposites, it was shown that the balance of entropic repulsion and enthalpic attraction may lead to string-like structures in some cases, even though interactions are nominally isotropic.[61–64] Note in particular that the curves for aggregated gels in Figure 3 are relatively similar to those observed in aggregated nanocomposites in ref.[64] Locally anisotropic interactions leading to string-like aggregation may also result from non-uniform polymer adsorption. Assessing this hypothesis, however, would require additional work, beyond the present study.

Measurements conducted on several samples showed a relatively large dispersion in the aggregation state, which reflects the difficulty to control the dispersion state using redox-initiated Free Radical Polymerization, as already mentionned in Section 3.1. As polymerization starts almost instantaneously at low pH, it is difficult to inject the sample in capillaries before gelation occurs. Perfect control of the aggregation state would certainly require further investigation.

3.3 Swelling behavior and extractible content

Equilibrium swelling measurements were done to assess that the polymerization process was not significantly affected by changing the pH. In all samples, the values of the extractible contents remain very low (smaller than about 2%), as reported in Table 3. This shows that the change of silica surface induced by changing the pH does not significantly impact the polymer network topology. Dynamic light scattering analyses of the solvent washed out from samples at swelling equilibrium did not reveal any leakage of silica nanoparticles, when the samples were able to withstand the osmotic pressure.

Table 3: Swelling properties of hydrogels. Q_0 and Q_e are the swelling ratios in the initial (preparation) state and at swelling equilibrium respectively, calculated from Eqs. 1 and 2.

Nomenclature	Q_0	Q_e	$S_R = Q_e/Q_0$	extractible (wt%)
MD	8.45	50 ± 8	5.9 ± 1	0.74
MA	11.34	76 ± 10	7 ± 1	1.12
NC_D	8.45	29 ± 8	3.4 ± 1	1.81
NC_A	11.34	193 ± 30	17 ± 3	1.96
NC_D_ag	8.45	33 ± 8	3.9 ± 1	1.51
NC_A_ag	11.34	301 ± 40	27 ± 3	1.78

The NC_D sample shows a decreased equilibrium swelling as compared to the unfilled MD gel. This is due to the presence of adsorption layers at the surface of nanoparticles, which restricts the swelling ability.[65] The NC_D_ag sample has a slightly increased equilibrium swelling (that is, a decreased restriction to swelling) as compared to NC_D. This is somehow unexpected, since silanol groups at the silica surface are supposed to favor attractive interactions with PDMA. The difference may perhaps be attributed to a lowered specific surface available for polymer adsorption due to the aggregation state of silica NPs.

The NC_A sample shows much higher equilibrium swelling as compared to MA. For a non interacting polymer, depletion zones or cavities around nanoparticles appear in the swollen state, which increases the overall macroscopic swelling[65]. Such cavities may act as fracture initiators and lead to inability to withstand osmotic pressure. Indeed, the NC_A_ag test samples show extremely high equilibrium swelling, leading sometimes to their disintegration and

to the leaking out of nanoparticles. This also shows that particle aggregates may dissociate under osmotic stress.

3.4 Mechanical properties

3.4.1 Tensile behavior

The results of tensile tests carried out at 0.06 s^{-1} are shown in Figure 4 for well-dispersed and aggregated hybrid gels. The behavior of hybrid gels based either on PAAm or PDMA differs considerably.

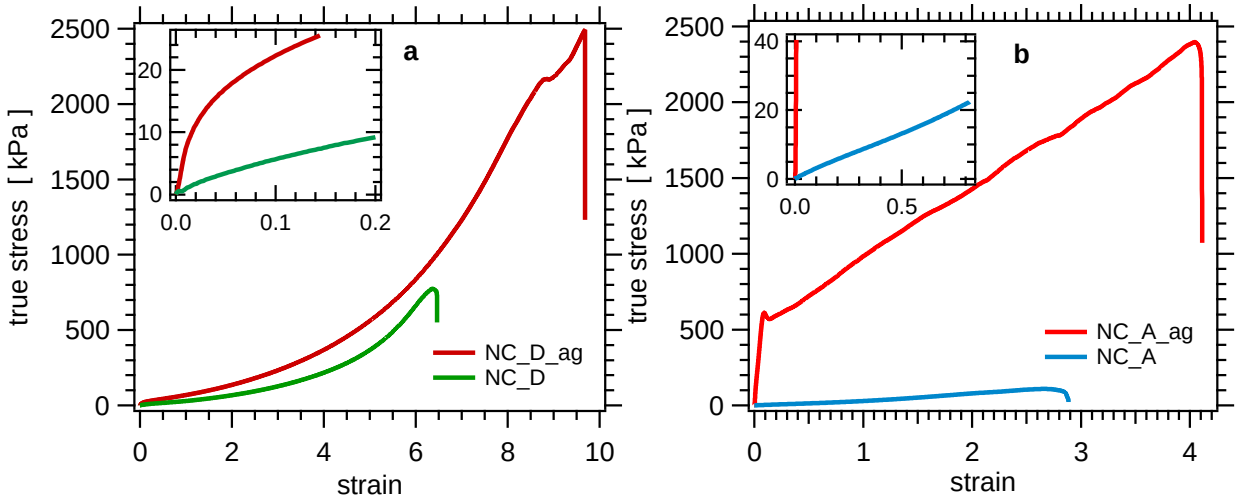

Figure 4: Stress-strain tensile curves of: **a**: NC_D and NC_D_ag; **b**: NC_A and NC_A_ag. Tests were conducted at 0.06 s^{-1}. The silica volume fraction is 0.2 for all samples. Insets are zooms of the curves at small strain values.

For PDMA-based samples, the general shape of the NC_D_ag tensile curve is similar to the one of the reference system NC_D (Figure 4 a), with a sigmoidal shape. NC_D_ag gels, however, are much stiffer than their counterparts with well-dispersed silica. Besides, the non-linearity, that is, the drop of modulus, analogous to the Payne effect observed in reinforced elastomers,[30,66,67] is much more pronounced, as shown in the inset in Figure 4 a. This behavior indicates that aggregation of silica nanoparticles provides a stiff network which then breaks as the stress increases. Strain softening at intermediate strain and strain

hardening at large strain indicate that, even though silica is aggregated, the dynamics of reversible interactions are still at play in those systems. As already observed in SAXS experiments, the aggregation state of the nanoparticles can largely vary between tested samples, with large variations of the experimental values of the linear tensile modulus (as reported in Table 4) and of the strain at break (from 500% to 1000 %). This, again, reflects the difficulty in controlling the aggregation state.

In NC_A samples (Figure 4 b), no strain softening at intermediate strain nor strain hardening at higher strain is observed. The behavior is qualitatively comparable to that of the unfilled matrix, with a higher modulus however. Silica nanoparticles thus do not bring typical patterns of reinforced materials, which is consistent with the presence of a non-interacting polymer matrix. NC_A_ag samples exhibit inhomogeneous deformation, with striction patterns for some samples. The linear tensile modulus values are unusually high for hydrogels (of the order of MPa) but largely vary among test samples. The behavior at small strain is fully driven by a hard network of aggregated particles (see inset in Figure 4 **b**), which breaks at small strain values.

3.4.2 Dissipative processes and recovery

The response of PDMA-based samples under cyclic tensile loading is shown in Figure 5. Deformation remains homogeneous throughout the stretching process. The samples are initially stiff and opaque while they become transparent during elongation. This gives a first qualitative indication that silica aggregates break under elongation. As already noticed, in the linear regime, the tensile modulus is much higher for NC_D_ag than for NC_D (Figure 5 a). Besides, NC_D_ag shows a larger hysteresis than NC_D. The linear tensile modulus drops considerably when a second cycle is performed without delay, similar to the Mullins effect observed in reinforced elastomers.[68] The drop of modulus is also associated to residual deformation, i.e. to some degree of instantaneous plasticity. However, after a short time of rest (30 seconds), NC_D shows full recovery of the modulus and of the residual deformation,

while this is not the case for NC_D_ag, which has a recovery ratio R (defined as the ratio of the linear tensile modulus of the second cycle over the modulus of the first cycle) of 0.33 for NC_D_ag against 0.98 for NC_D. In NC_D_ag, successive cycling up to increasing strain values (from 20 to 200%) shows instant damage with a drastic decrease of the initial modulus between each cycle ($\approx$ 90% between the first and the last cycle) and large residual strain (Figure 5b). However, full recovery of the mechanical response is observed after a 24 hour rest, as shown in Figure 5b.

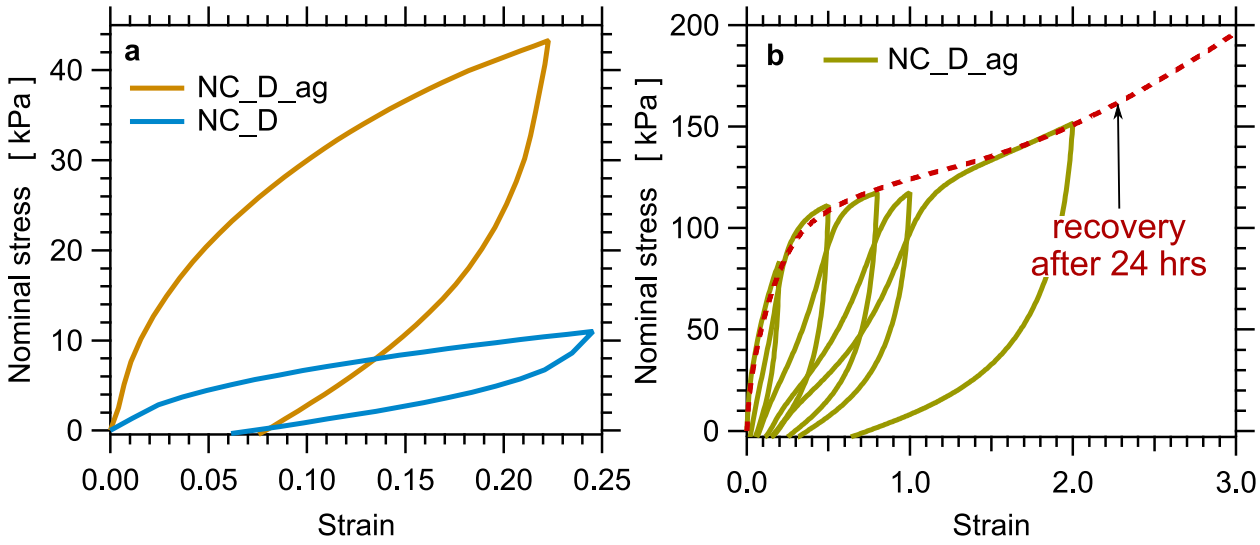

Figure 5: **a**: Tensile cycles of NC_D and NC_D_ag up to 25% and 20% strain respectively. **b**: Successive tensile cycles of NC_D_ag up to increasing maximum strain values (20, 50, 80, 100 and 200%), followed by a tensile test performed 24 hours after the cycles (dashed red curve) which shows the full recovery of the mechanical response. All tests were conducted at 0.06 s^{-1}.

Table 4: Linear tensile modulus (E) and mechanical recovery parameters measured after a 30 s (R_{30s}) or 24 hour (R_{24h}) delay. The recovery parameter R is defined as the ratio of the modulus of the second cycle or tensile test over the modulus of the first cycle (amplitude of the first cycle 25%). The strain rate is $\dot{\epsilon} = 0.06$ s^{-1}.

Sample	NC_D	NC_A	NC_D_ag	NC_A_ag
E (kPa)	92 ± 8	23 ± 4	730 ± 25	5000 ± 2500
R_{30s}	0.97	0.88	0.33	0.57
R_{24h}	~ 1	~ 1	1.14	0.05

NC_A_ag samples as well show considerable hysteresis, quite large plasticity and a drastic

decrease of the mechanical response between the first and second cycles, as shown in Figure 6a. The dissipated energy during the first load is even higher than that of NC_D_ag, which may be related to a higher level of nanoparticle aggregation. As PAAm does not interact with silica, reinforcement in NC_A_ag should be driven by the hard silica network only. Contrary to what happens in the NC_D_ag sample, the mechanical behavior is not recovered after 24 hour rest, as shown in Figure 6b. This emphasizes the absence of interactions and the irreversibility of the damage undergone by the sample. In these samples, the deformation is inhomogeneous, indicating a yielding phenomenon, with zones that remain turbid while other ones turn transparent, due to previous deformations during the loading cycles.

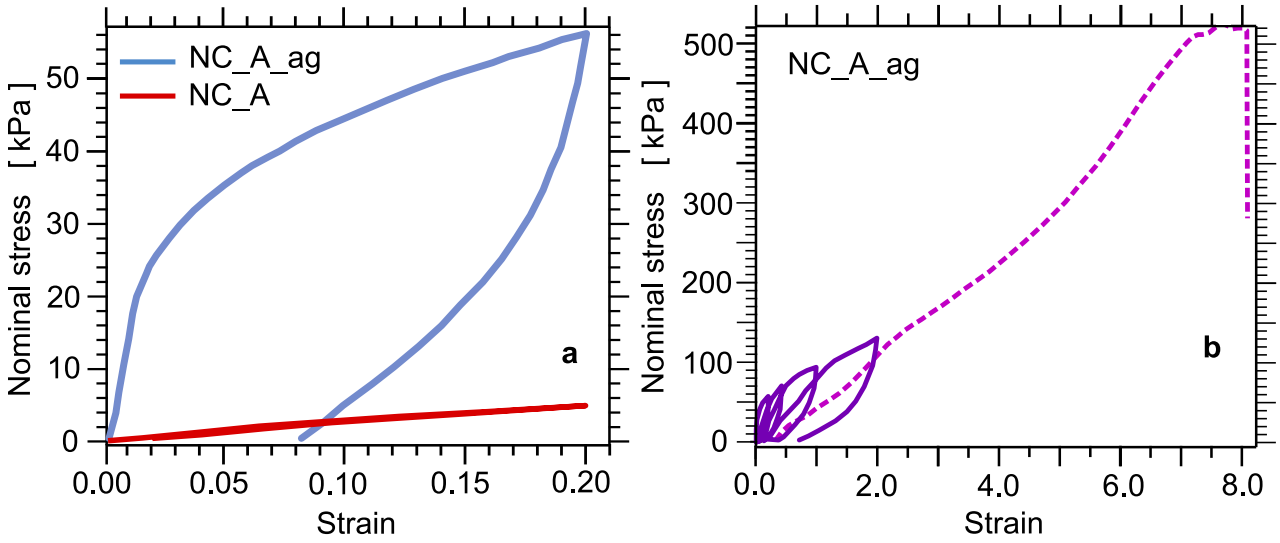

Figure 6: **a**: Tensile cycles of NC_A and NC_A_ag up to 20% strain. **b**: Successive tensile cycles of NC_A_ag up to increasing maximum strain values (20, 50, 80, 100 and 200%), followed by a tensile test performed 24 hours after the cycles (dashed red curve). All tests were conducted at 0.06 s^{-1}.

3.5 Large Amplitude Oscillatory Shear (LAOS)

3.5.1 Unfilled gels

Raw stress-strain data (Lissajous curves) of oscillatory shear measurements for the unfilled PDMA- (MD) and PAAm-based (MA) gels are shown in Figure 7 at strain amplitudes varying from 3% to 65%.

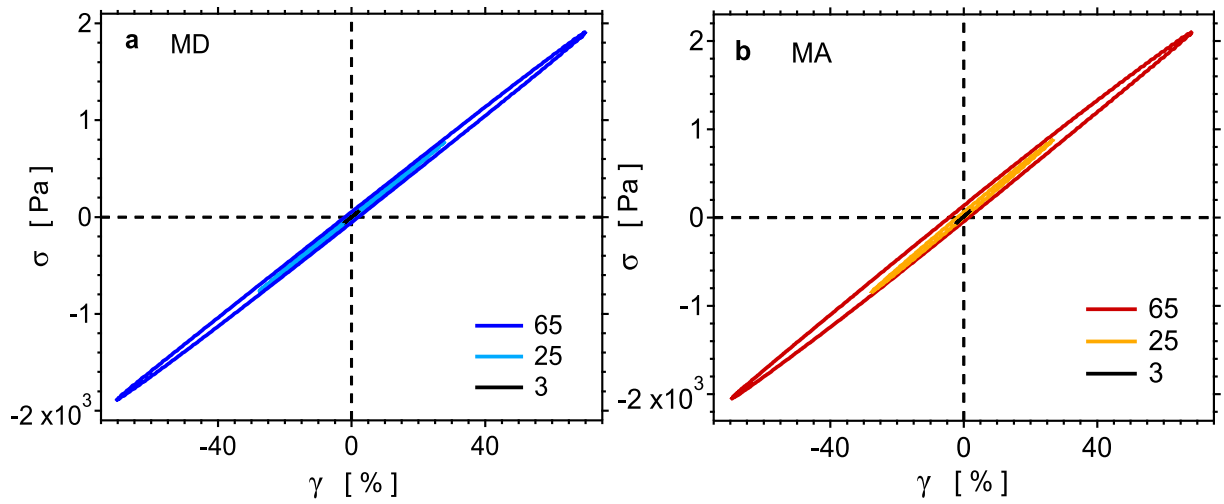

Figure 7: Lissajous curves at various maximum strain amplitudes as indicated in the legend (in %): **a**: MD gel; **b**: MA gel. The measurement frequency is 1 Hz.

The Lissajous curves of both MD and MA gels show linear behavior up to quite high strain amplitudes (up to 70% strain amplitude typically). The dissipation is very small, with G' typically 30 times larger than G''. The dissipation is slightly larger for MA than for MD, however. Altogether, unfilled gels have similar mechanical properties, independently of the chemical nature of the monomer.

3.5.2 LAOS experiments on well-dispersed hybrid gels

The mechanical properties of hybrid gels were first measured in the viscoelastic linear regime as a function of the frequency to specifically investigate the impact of the presence of the nanoparticles on the dynamic moduli. Results are shown in Figure 8.

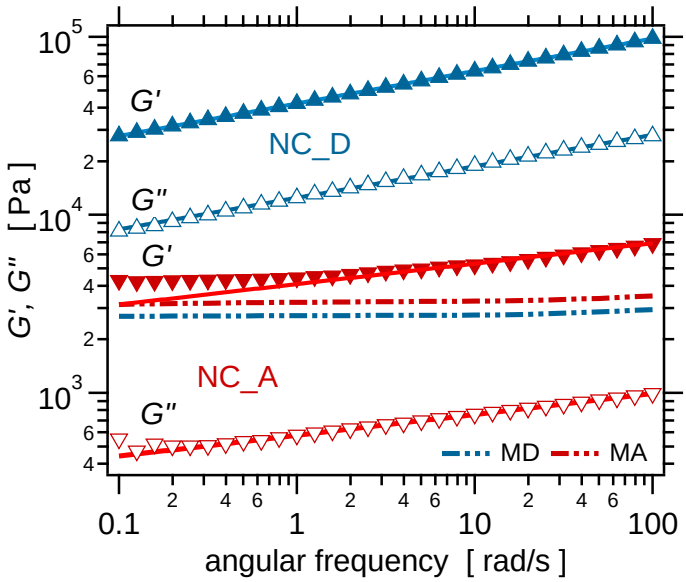

Figure 8: The storage (G', filled symbols) and loss (G'', open symbols) shear moduli of hybrid PDMA (blue) and PAAm (red) as a function of the angular frequency at oscillation strain amplitude 0.1%. The storage moduli of the unfilled MD (blue) and MA (red) gels are shown as dot-dashed curves for comparison. The loss moduli of MD and MA are of the order roughly 50 Pa, i.e. well below the range covered in the graph. Plain lines are fits with power laws of the form ω^{α} (see Table S1 in **SI**).

For NC_D gels (blue symbols in Figure 8), introducing silica nanoparticles leads to a large increase of G' but also of the frequency dependence as compared to the corresponding unfilled (MD) gel (blue curve). G'' also increases considerably, from less than 100 Pa for MD up to a few 10^4 Pa at 100 rad.s^{-1} for NC_D. Both G' and G'' follow an apparent power-law frequency response, similar to the one reported for physical gels[69–71] or hydrophobically-modified systems[72]. The fits of G' and G" with a power law ω^{α} with $\alpha = 0.18 \pm 0.003$ are shown in Figure 8. Thus, these measurements do not enable defining a characteristic time that would correspond to a maximum in the loss modulus, perhaps indicating that there is a large distribution of PDMA segments more or less adsorbed to the silica surface by one or more sites, giving a wide range of characteristics relaxation times.

The behavior of NC_A gels is different (red symbols in Figure 8). The enhancement of the dynamic modulus is much weaker and the frequency dependence is comparatively less pronounced, especially for G' (the power laws for G' and G'' indicated in Figure 8 are

$\omega^{0.117}$). G' shows a low-frequency plateau. This is a key figure of the response of this sample, as it indicates that the response is driven by the cross-link network, while dynamical polymer/filler interactions do not contribute to the modulus to the same extent as in the NC_D gel. The measured plateau value is of the order 5 kPa, which is close to the value expected from hydrodynamic, Guth and Gold-like reinforcement obtained from the value $\sim$ 3 kPa of the unfilled MA sample.[19] From this value, a characteristic mesh size of the network can then be roughly estimated using the classical expression from rubber elasticity $G \approx k_B T/\xi^3$. The value $\xi \approx 10$ nm is obtained, which is fully consistent with values reported for similar hydrogel systems.[73]

The behavior at large shear amplitudes at frequency 1 Hz (angular frequency 6.28 rad.s^{-1}) was then investigated. The Lissajous curves of NC_D and NC_A hybrid gels are shown in Figure S1 in **SI** for various strain amplitudes varying from 4% to 130%. For NC_D, two distinct non-linear phenomena are observed at large strain amplitudes: the ellipse is strongly distorted, with intra-cycle strain-stiffening, and the slope at the origin decreases as the strain amplitude increases, that can be paralleled to the Payne effect observed in filled rubbers.[7,30,66]

The NC_A gel shows much less pronounced non-linearities. Namely, the drop of the slope is less pronounced and no apparent strain-stiffening is present. This highlights once more the impact of the nature of the monomer-particle interactions on the mechanical behavior of hybrid gels.

The decompositions into elastic and viscous parts (as described in Section 2.4) are shown in Figure 9 for the NC_D sample for strain amplitudes varying up to 800% (see also Figure S2 in **SI**).

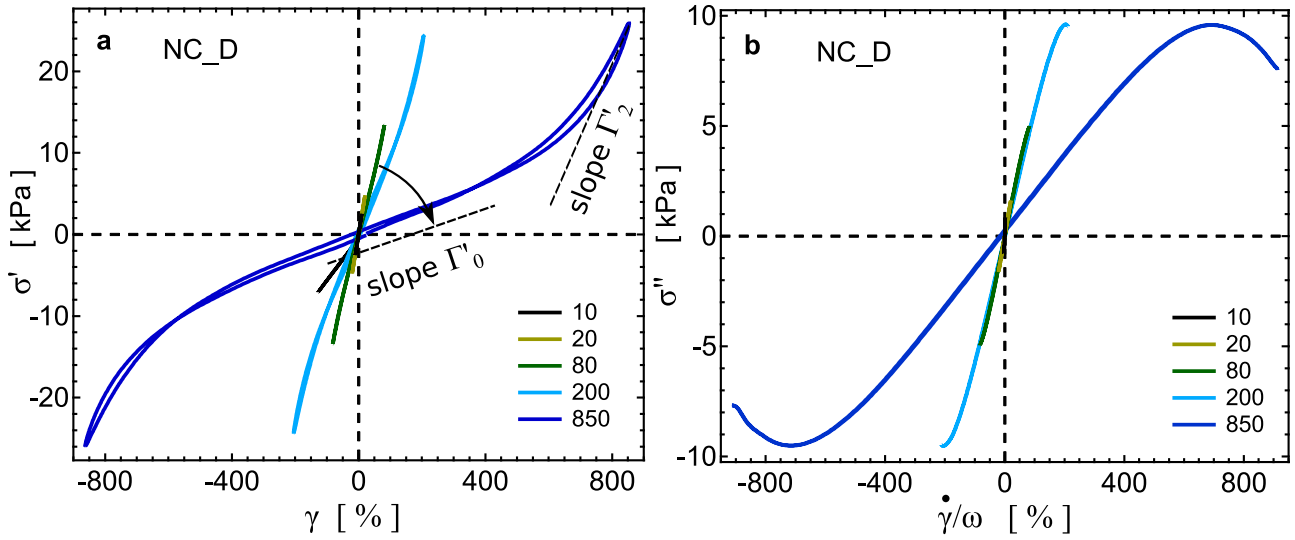

Figure 9: **a.** Decomposition into the odd (σ', elastic, **a**) and even (σ'', viscous, **b**) parts of the stress according to Equations 4 and 5, for various strain amplitudes (as indicated in the legends, in %), for the NC_D sample (obtained from data like those in Figure S1). The definitions of Γ'_0 and Γ'_2 are schematized in **a**. The arrow indicates the decrease of the modulus Γ'_0 as the strain amplitude increases. The small apparent hysteresis observed in the σ' cycles is an artifact due to imperfect strain regulation by the rheometer.

The evolutions of the storage and loss moduli are first described. Up to 100% strain amplitude, G' and G'' (as returned from the rheometer) nearly coincide with the slopes at origin Γ'_0 and Γ''_0 respectively, as non linearities are not that much pronounced and in fact correspond to small non-linear terms. The evolutions of G' and G'' as a function of the strain amplitude during increasing and decreasing amplitude sweeps for NC_D and NC_A are shown in Figure 10.

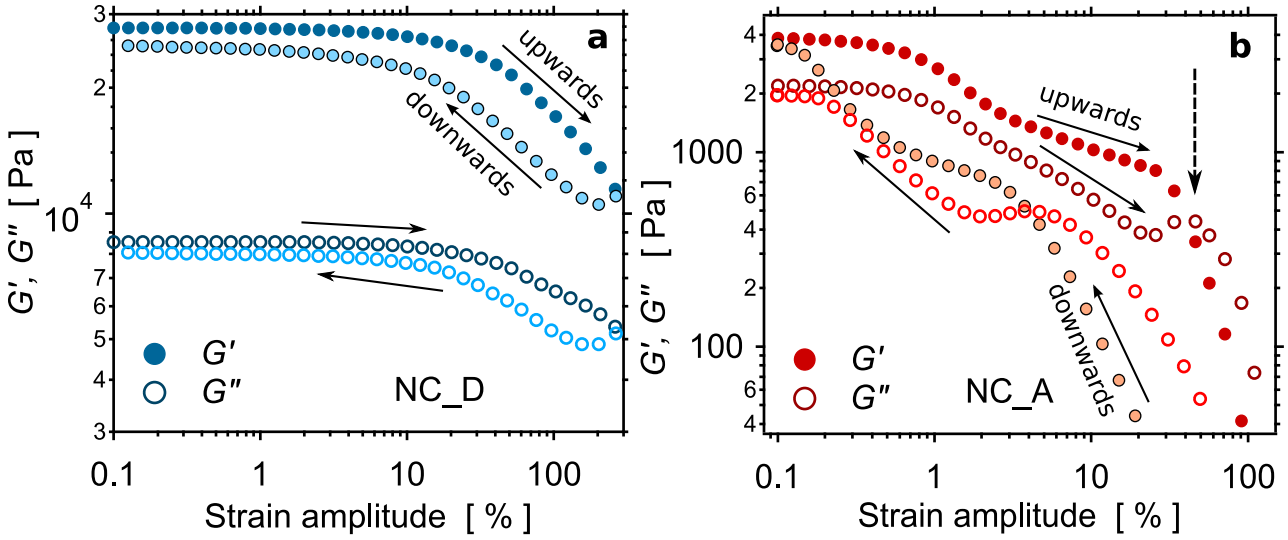

Figure 10: Storage (filled disks) and loss (empty circles) moduli of NC_D (**a**) and NC_A (**b**) as a function of the strain amplitude, during upwards and backwards amplitude sweeps from 0.1 to 250 % strain (without time of rest). The vertical dashed arrow in **b** indicate probable slippage or fracture of NC_A above 60 % strain amplitude.

For NC_D, at strain values smaller than about 10%, both G' and G'' remain constant indicating that the samples are still in the linear domain. At higher strain (around 20 %), G' and G'' start to decrease as the strain amplitude increases, with a more pronounced effect on the storage modulus, which is very similar to the Payne effect observed in filled rubbers, to the difference that this effect (usually observed between 1 and 10 % of strain amplitude in filled elastomers[7,74]) seems to be shifted towards higher strain values. Note that the loss modulus does not show a maximum as the strain amplitude increases, as is commonly observed in filled rubbers. The ratio G''/G' stays nearly constant up to nearly 20% strain and then increases.

NC_A samples behave slightly differently, with multi-step yielding, that is, two successive drops of modulus, one first drop occurring at strain amplitudes between 0.1 and 1%, very similar to what is observed in filled rubbers, followed by a pseudo-plateau at intermediate strain amplitudes between 1 and 25 %. Around 25% strain, dynamic moduli drop further, with a more pronounced, very steep decay for the storage modulus, even more pronounced than what is observed for NC_D. This second decay should be eventually related to the

breakup of silica clusters or network.

LAOS data for the NC_A sample decomposed into elastic and viscous parts are shown in Figure S2 in **SI**. As mentionned above (see Figure 9), strain hardening occurs within a given cycle, concomitantly to the drop of modulus. As NC_D has a much higher stretching ability than NC_A, its response was measured at much higher strain values.

In the high strain regime, for the NC_D sample, the non-linearities become even more pronounced. A marked strain-stiffening ($\Gamma'_2 > \Gamma'_0$ within one strain cycle) is observed at high strain amplitudes. A strain-hardening parameter may be defined as the ratio $\Gamma'_2(\gamma_0)/\Gamma'_0(\gamma_0 = 0)$. This ratio is shown in Figure 11 as a function of the strain amplitude for both NC_D and NC_A gels. NC_A gels show no significant difference between Γ'_0 and Γ'_2, with a strain-hardening ratio close to one up to strain amplitudes of order 150%. In those systems, the non-linearity of the behavior is reflected in the drop of the Γ'_0 modulus only. In NC_D gels, strain hardening starts to be observable between 20 and 60% and then increases steeply beyond about 100% strain amplitude.

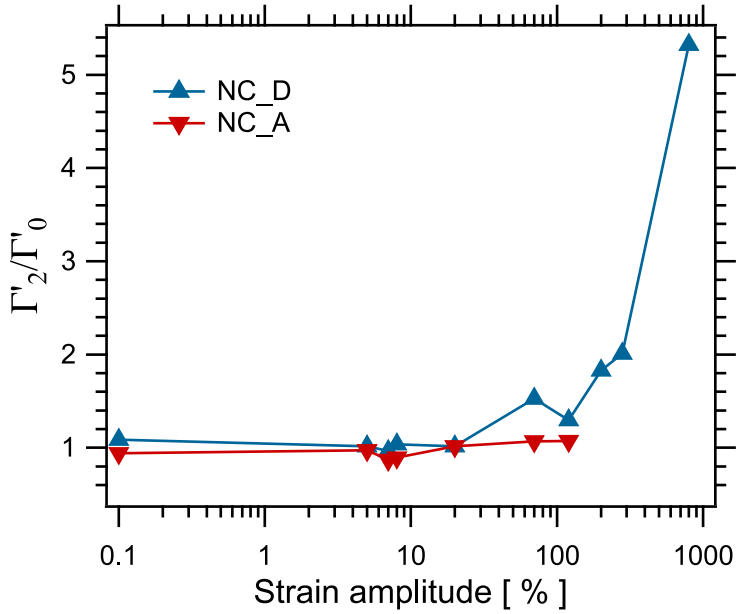

Figure 11: The strain-hardening parameter $\Gamma'_2(\gamma_0)/\Gamma'_0(\gamma_0 = 0)$ as a function of the strain amplitude γ_0 of NC_D and NC_A.

This ensemble of results confirms that the main contribution to reinforcement in well-

dispersed hybrid gels comes from reversible adsorption/desorption of polymer chains at silica surface. These interactions are also responsible for the pronounced non-linear behavior. Conversely, NC_A show both much weaker reinforcement and much less pronounced non-linearities, as shown in Figures 8, 9 and 11.

3.5.3 LAOS on hybrid gels with aggregated silica

The storage and loss moduli for NC_D_ag and NC_A_ag gels in the linear regime are shown in Figure 12 as a function of the frequency. For NC_D_ag gels, aggregation of silica nanoparticles leads to an increase of G' and G'' and of the frequency dependence, similarly to what is observed for ND_D gels, with higher modulus values however. Both G' and G'' follow an apparent power-law frequency response similar to the one reported for physical gels[69–71] or hydrophobically-modified systems[72]. These measurements indicate that there is a large distribution of relaxation times.[3]

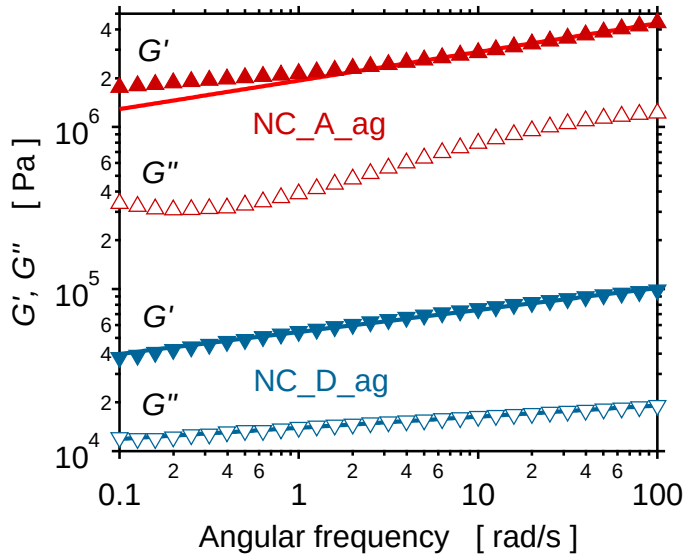

Figure 12: **a.** The storage (G',filled symbols) and loss (G'', open symbols) moduli of PDMA (NC_D_ag, blue symbols) and PAAm (NC_A_ag, red symbols) hybrid gels as a function of the angular frequency, at strain amplitude 0.1%. Blue (resp. red) plain lines are fits of NC_D_ag data (resp. NC_A_ag storage modulus) with power laws of the form ω^{α} (see Table S1 in **SI**).

The NC_A gels show a slightly different behavior, with a much higher dynamic modulus, in the MPa range. G'' seems to slightly decrease first, before increasing as the frequency increases, which could be due to the hard filler network response. A maximum in $\tan\delta$ is observed at about 60 rad.s^{-1}. The Young's modulus values calculated from rheology experiments and determined from uniaxial tensile tests (such as those shown in Figure 4) at low strain are reported in Table S1 in **SI**. Both values coincide well, which confirms the coherence of all measurements.

The instantaneous elastic and viscous components of the stress for NC_D_ag are shown in Figure S3 in **SI** as a function of the strain for various maximum strain amplitudes up to the non-linear regime. Non-linear effects are even more pronounced, with a strong deviation from the linear behavior occurring at lower strain amplitude, than for NC_D. The drop in modulus (Figure 13) seems to show two successive steps, as indicated by dashed red vertical arrows in Figure 13. The first drop occurs at around 1% strain amplitude. It is similar to what is observed in filled rubbers and might be attributed to the breaking of the silica network (which is responsible for the enhancement of the dynamic modulus by about two orders of magnitude as compared to the corresponding unfilled gel). The second step of decrease (around 50% strain amplitude) is similar to what is observed in the NC_D gels and may be attributed to partial desorption of polymer chains. G'' also decreases, but more smoothly than its elastic counterpart. A drop of modulus values is observed when comparing upwards and downwards sweeps. This is consistent with the behavior observed in tensile tests (see Figure 5), in which a drop of the mechanical response was also observed when the second test is performed without delay. On the other hand, it was shown that the mechanical behavior is fully recovered after a 24h delay (Figure 5b).

Another interesting feature in Figure 13 is the further decrease of apparent moduli at the start of the downwards sweep. This indicates the presence of structural changes and/or local breakup and reorganization of the silica network with some retardation delay, which emphasizes once more the importance of kinetic aspects.

Strain-stiffening within one cycle increases as the strain amplitude increases. The non-linear parameter $\Gamma'_2\ (\gamma_0)/\Gamma'_0\ (\gamma_0 = 0)$ is plotted in figure 14 as a function of the strain amplitude for NC_D and NC_D_ag samples. Strain-stiffening is more pronounced when silica is aggregated. This might be due to the finite extensibility of adsorbed polymer chains onto the silica clusters but also to the presence of anisotropic silica aggregates.

Γ''_2 stays positive up to $\approx 60\%$ strain then becomes negative, pointing to shear-thinning of the sample.

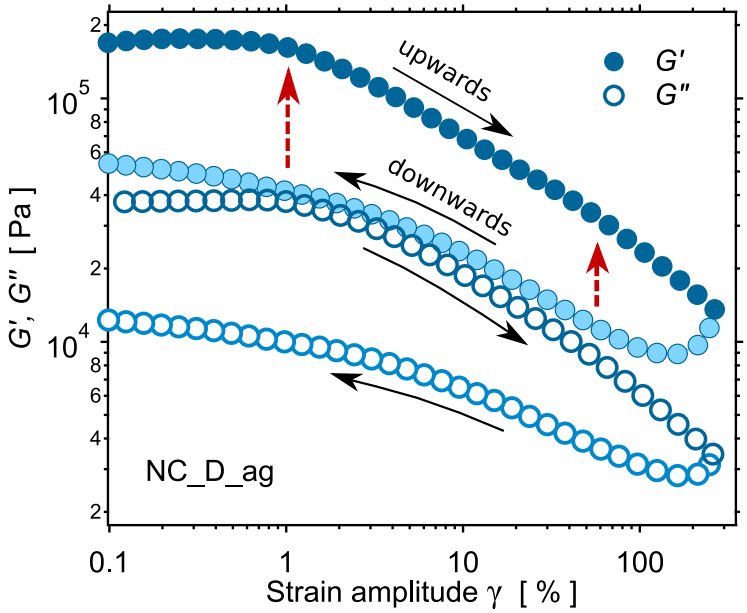

Figure 13: Storage (filled symbols) and loss modulus (empty symbols) of NC_D_ag as a function of the oscillating strain amplitude, during upwards and downwards amplitude sweeps (as indicated by black arrows) up to 400% performed without time of rest, at frequency 1 Hz. Red dashed vertical arrows roughly indicate the onsets of successive decay steps.

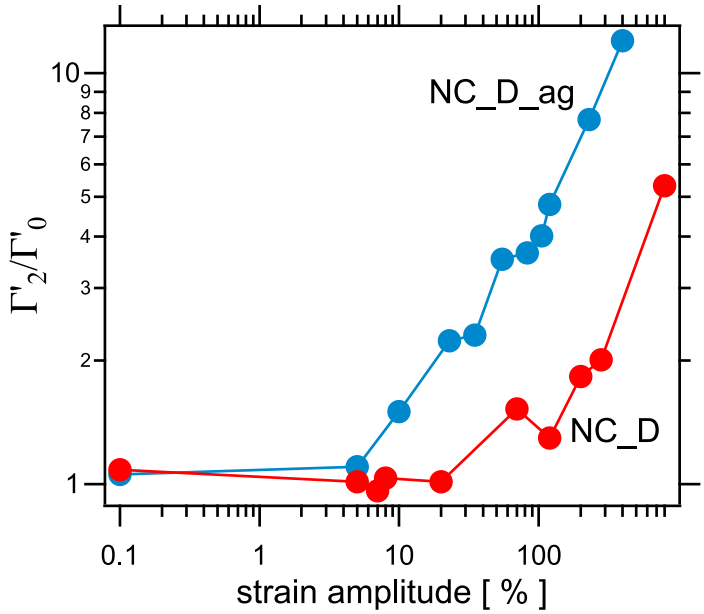

Figure 14: Non-linear parameter Γ'_2 $(\gamma_0)/\Gamma'_0$ $(\gamma_0 = 0)$ as a function of the strain amplitude γ_0 (%) of NC_D (blue) and NC_D_ag (orange).

The elastic and viscous components of the stress for NC_A_ag are shown in Figure S4 in **SI**. Note that the range of strain amplitudes is much lower than in Figure S3. The slope Γ'_0 starts to decrease at maximum strain amplitudes lower than 1 % (G' decreases by 10% at 0.5% of strain), as shown in Figure 15. The drop of the dynamic moduli is larger than for NC_D_ag at the same level of deformation (Figure 15). At these strain values, however, the other features of non-linearity (strain-stiffening or shear-thinning) are not very pronounced. As the strain amplitude increases beyond 10% typically, both G' and G'' drop quite abruptly, as shown in Figure 15, which indicates that NC_A_ag samples undergo permanent damage.

The values of the dynamic moduli are initially very high (of the order of 2 MPa for G'). Conversely, PAAm hybrid gels with well-dispersed silica do not show strong reinforcement, with G' values of the order of a few 10^3 Pa, due to the absence of polymer/filler interactions as a reinforcement mechanism (see Figure 8). The more likely hypothesis is then that silica nanoparticles strongly aggregate during the polymerization of AAm, leading to a hard percolating silica network that irreversibly breaks under the shear, whatever the resting time allocated, explaining both the very high modulus obtained for those gels and the observed

damages.

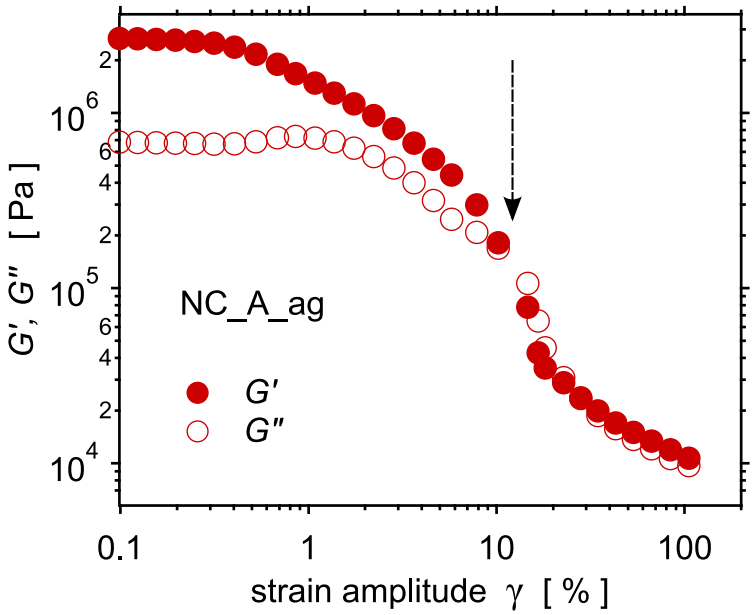

Figure 15: Storage and loss moduli of NC_A_ag at frequency 1 Hz as a function of the strain amplitude from 0.1 to 100 % . The vertical dashed arrow indicates the occurrence of damage at about 10% strain.

The non-linear parameter $\Gamma'_2\ (\gamma_0)/\Gamma'_0(\gamma_0 = 0)$ for NC_A_ag samples is shown in Figure 17. The non-linear effects are even stronger than in of NC_D_ag samples at the same strain amplitude, underlying the fact that stronger silica aggregation leads to pronounced non-linearity.

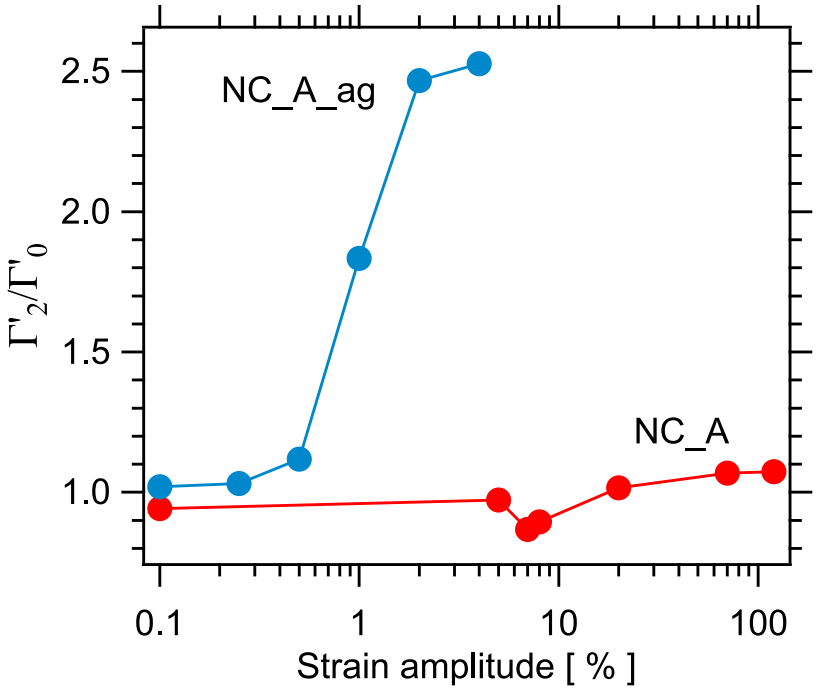

Figure 16: The non linear parameter $\Gamma'_2\ (\gamma_0)/\Gamma'_0(\gamma_0 = 0)$ of NC_A_ag (blue symbols) as a function of the strain amplitude γ_0. The non linear parameter of NC_A is also shown (red) for comparison.

3.5.4 Recovery properties

Recovery processes were investigated in the NC_D_ag sample by performing successive strain amplitude sweeps, first without rest time (from 0.1 to 250% then from 250% to 1%), then after 24 hours rest (from 1 to 250 %). Results are illustrated in Figure 17 (see also Figure 13).

Right after the first amplitude sweep, the sample seems to be permanently damaged compared to NC_D (Figure 10 a), with a recovery parameter not exceeding 0.32 at small strains. However, after 24 hours of rest, the sample seems to have fully recovered his viscoelastic response. The obtained G' remains a little smaller, while G'' is slightly above, than during the first amplitude strain sweep, which indicates that the sample undergoes polymer/silica rearrangement after stretching. These experiments confirm the recovery properties of NC_D samples observed in tensile tests, as discussed in Section 3.4.2.

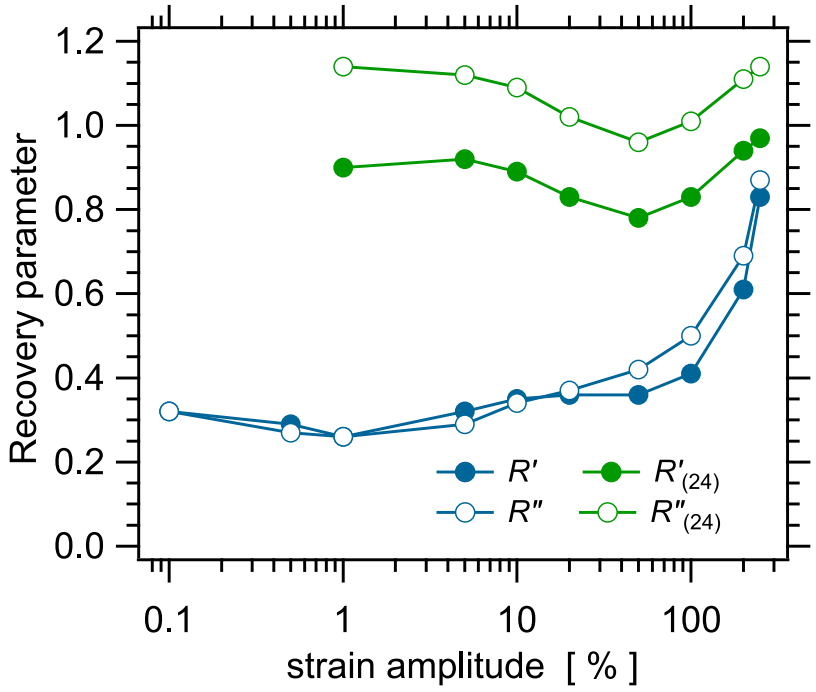

Figure 17: Recovery parameters $R' = G'_{(1)}/G'_{(2)}$ for the NC_D_ag sample, where $G'_{(1)}$ and $G'_{(2)}$ are the moduli measured during the first (upwards) and second (downwards) strain amplitude sweeps respectively and $R'_{(24)} = G'_{(1)}/G'_{(24)}$ where $G'_{(24)}$ is the modulus measured during the second (upwards) strain amplitude sweep performed after 24 hours. Recovery parameters R'' are defined in a similar way with G'' values.

3.6 Discussion

The observed behavior indicates that the response of the material changes in the whole strain range depending on the maximum strain amplitude. It cannot be described by a non-linear hyper-viscoelastic constitutive equation relating σ to γ and/or $\dot{\gamma}$. This would be the case for example if strain hardening was due to finite extensibility of gel network chains alone. In such a hyperelastic material, the σ' vs γ curves obtained at various maximum strain amplitudes would superpose in their common regime. This behavior has strong similarities with the characteristic behavior of elastomers reinforced by nanoparticles, with different orders of magnitude for the modulus however[35,40]. In reinforced elastomers, the network of rigid polymer bridges (so-called glassy bridges) that connect neighboring filler particles plays a key role in reinforcement.[75,76] In that context, the non-linear behavior was modeled

by considering the kinetics of yielding/reformation of glassy bridges.[77,78] Specifically, a new non-linear mechanism denoted 'slowing-down-hardening' was proposed[40]. In an oscillatory strain cycle, the strain rate goes down to zero at the maximum strain, which gives more time for glassy bridges to reform. It follows that more glassy bridges contribute to the modulus at the maximum of a cycle. Of course, no glassy bridges are present in gels. It may be proposed, however, that the kinetics of adsorption/desorption of polymer chains on silica nanoparticles may result in a qualitatively similar behavior. Applying a large amplitude strain may affect the polymer/filler adsorption/desorption dynamics, which may explain the drop of modulus. Then, as the strain rate goes to zero at the maximum strain in a cycle, chain segments may have more time to re-adsorb, which may lead to the observed apparent strain hardening. As regards the viscous contribution (Figure 9 b), σ'' reaches a maximum during each cycle at some intermediate strain amplitude. This phenomenon was also observed and modelled in filled elastomers as a consequence of the complex yielding/reformation kinetics of glassy bridges[40]. The same kinetic balance may be at play in PDMA hybrid gels with the adsorption/desorption dynamics. This hypothesis would explain as well that strain hardening is not present in NC_A, in which chain adsorption is weak.

Regarding the impact of silica nanoparticle aggregation, several, distinct effects may influence the mechanical response. In NC_D_ag gels, silica aggregation may decrease the silica surface available for polymer adsorption. On the other hand, at the acid pH used to synthetized these gels, the density of silanol groups at silica surface is higher than at pH 9[54], which should favor polymer/silica interactions.

The proposed hybrid networks with aggregated particles also have strong similarities with so called 'attractive colloids' or 'arrested phase separation gels', which shows both a marked yield stress, thixotropy and ageing.[79] In our case, the phase separation (i.e. silica aggregation) may be arrested at some (hopefully controlled) stage by the crosslinking of the polymer network. While, referring to the decrease of mechanical properties at short term, our materials indeed show thixotropy, ageing leads to a nearly complete recovery of

the properties in PDMA hybrid gels. The present study illustrates the key role of polymer-particle interactions in this recovery.

The silica network with reinforced polymer-silica interactions may provide the high modulus during the initial stage of the load. The silica network then breaks at higher strain, giving high energy dissipation. The silica network may then be restored after some time, which indicates that reversible interactions between PDMA and silica still take place, but at a longer time scale, and are essential to explain recovery properties. Reorganisation of silica clusters could also be involved in the long-time scale of recovery.

At an equivalent strain value, strain-stiffening is larger for NC_D than for NC_A samples. This means that strain-stiffening does not only come from non-linear dissipation, which is present in both samples. It may also be affected by local strain amplification and finite extensibility of polymer chains confined between chemical cross-links and silica nanoparticles that act as supplementary cross-link points. The presence of depletion layers in NC_A samples may enable slippage of the polymer matrix at the surface of the particles, which would decrease the local strain amplification as compared to NC_D samples. This might also explain why the modulus drops earlier in the case of NC_A (8 % strain to reach a 10% decrease of initial storage modulus of NC_A against 15% strain for NC_D).

Finally this work opens potential developments to rationalize the mechanical response of the silica network formed in aggregated samples and the ageing/recovery properties more thoroughly. Stress-controlled experiments and systematic studies of the kinetics of ageing/recovery as a function of the applied stress,[80] together with in-situ structural studies of the non-linear deformation processes,[81] may certainly be of high interest.

4 Conclusion

The surface chemistry of silica nanoparticles was tuned in order to promote aggregation in PDMA (denoted NC_D) and PAAm (NC_A) hybrid hydrogels. The behavior of hybrid gels

with aggregated nanoparticles (denoted _ag) is completely different from those where silica is well-dispersed within the matrix. NC_D_ag hybrid gels display marked non-linear behavior, similar to those observed in filled elastomers, with strong strain stiffening along with large dissipation. In NC_D_ag, reinforcement can be attributed to two specific features: (1) reversible interactions between PDMA and silica nanoparticles, that provide strain-stiffening and recovery, and (2) silica aggregation, that leads to enhanced stiffness, dissipative processes and pronounced strain-stiffening effects. Recovery processes observed in NC_D are preserved, but the characteristic time needed to fully recover is eventually extended from a few seconds to several hours. In those gels, reinforcement is certainly related to the nanoparticle dispersion state but also to reversible interactions that seem to be still effective, even though silica forms clusters. The observed recovery may perhaps be favored by the higher density of silanol groups at the silica surface due to the change in surface chemistry, that would strengthen the interactions with the polymer. Coming back to the notion of sacrificial network, reorganization of the silica particle network, before it finally breaks, may provide the efficient dissipation mechanism suitable to enhance the toughness of the materials. The present study further shows that reversible polymer-silica interactions play a key role in the recovery of the mechanical properties in the case of PDMA-based systems.

For NC_A_ag hybrid gels, no recovery processes are observed. This implies that the properties, namely the very high linear tensile modulus and high dissipated energy, are driven by the rigid network formed by nanoparticle aggregation, that provides high dissipative capabilities, especially when compared to NC_A gels, that remain soft and fragile. These gels exhibit a quite inhomogeneous structure with permanent damage under elongation.

The non-linear dynamical behavior of hybrid gels was investigated by LAOS experiments. While unfilled gels show no non-linearity up to very large strain amplitude, marked non-linear effects combining a drop of modulus s (similar to the Payne effect) and strain-stiffening for increasing strain amplitude, are observed in NC_D, certainly due to polymer adsorption onto nanoparticles. NC_A samples also show non-linearity, with a drop of moduli for increasing

strain but no strain-stiffening, indicating that the presence of fillers alone can induce non-linearity in the absence of strong, reversible polymer-particle interactions. The analysis of the non-linear behavior indicates the importance of the kinetics of re-adsorption of polymer chains desorbed under large amplitude strain. In NC_A_ag samples, reinforcement is enhanced by silica aggregation, which leads to very high stiffness and high dissipative properties, at the expense of stretchability, though. Also, the structure seems to be permanently damaged under stress, revealing the importance of silica/polymer interactions for permanent mechanical reinforcement.

5 Supplementary information

- Large Amplitude Oscillatory Shear (LAOS) measurements
  - Obtaining raw data
  - Measurement results
- Values of the elastic moduli

References

(1) Li, H. J.; Jiang, H.; Haraguchi, K. Ultrastiff, Thermoresponsive Nanocomposite Hydrogels Composed of Ternary Polymer–Clay–Silica Networks. *Macromolecules* **2018**, *51*, 529–539.

(2) Carlsson, L.; Rose, S.; Hourdet, D.; Marcellan, A. Nano-hybrid self-crosslinked PDMA/silica hydrogels. *Soft Matter* **2010**, *6*, 3619–3631.

(3) Rose, S.; Dizeux, A.; Narita, T.; Hourdet, D.; Marcellan, A. Time Dependence of Dissipative and Recovery Processes in Nanohybrid Hydrogels. *Macromolecules* **2013**, *46*, 4095–4104.

(4) Rose, S.; Marcellan, A.; Hourdet, D.; Creton, C.; Narita, T. Dynamics of Hybrid Polyacrylamide Hydrogels Containing Silica Nanoparticles Studied by Dynamic Light Scattering. *Macromolecules* **2013**, *53*, 4567–4574.

(5) Rose, S.; Marcellan, A.; Narita, T.; Boue, F.; Cousin, F.; Hourdet, D. Structure investigation of nanohybrid PDMA/silica hydrogels at rest and under uniaxial deformation. *Soft Matter* **2015**, *11*, 5905–5917.

(6) Wang, M. J. Effect of Polymer Filler and Filler-Filler Interactions on Dynamic Properties of Filled Vulcanizates. *Rubber Chemistry and Technology* **1998**, *71*, 521–559.

(7) Chazeau, L.; Brown, J. D.; Yanyo, L. C.; Sternstein, S. S. Modulus Recovery Kinetics and Other Insights Into the Payne Effect for Filled Elastomers. *Polymer Composites* **2000**, *21*, 202–222.

(8) Heinrich, G.; Kluppel, M. Recent Advances in the Theory of Filler Networking in Elastomers. *Filled Elastomers Drug Delivery Systems* **2002**, *160*, 1–44.

(9) Haraguchi, K.; Takehisa, T.; Fan, S. Effects of Clay Content on the Properties of Nanocomposite Hydrogels Composed of Poly(N-isopropylacrylamide) and Clay. *Macromolecules* **2002**, *35*, 10162–10171.

(10) Haraguchi, K.; Takehisa, T. Nanocomposite hydrogels: A Unique Organic-Inorganic network Structure with Extraordinary Mechanical, Optical ans Swelling/Deswelling Properties. *Advanced Materials* **2002**, *14*, 1120–1124.

(11) Haraguchi, K.; Li, H. J. Control of the coil-to-globule transition and ultrahigh mechanical properties of PNIPA in nanocomposite hydrogels. *Angew Chem Int Ed Engl* **2005**, *40*, 6500–6504.

(12) Ronsin, O.; Naassaoui, I.; Marcellan, A.; Baumberger, T. Environmental Nanoparticle-

Induced Toughening and Pinning of a Growing Crack in a Biopolymer Hydrogel. *Physical Review Letters* **2019**, *123*, 158002.

(13) Rose, S.; Prevoteau, A.; Elziere, D., P.and Hourdet; Marcellan, A.; Leibler, L. Nanoparticle solutions as adhesives for gels and biological tissues. *Nature* **2014**, *505*, 382–385.

(14) Lion, A.; Kardelky, C.; Haupt, P. On the Frequency and Amplitude Dependence of the Payne Effect: Theory and Experiments. *Rubber Chemistry and Technology* **2003**, *76*, 533–547.

(15) Hofer, P.; Lion, A. Modelling of frequency- and amplitude-dependent material properties of filler-reinforced rubber. *Journal of the Mechanics and Physics of Solids* **2009**, *57*, 500–520.

(16) Berriot, J.; Montes, H.; Lequeux, F.; Long, D.; Sotta, P. Gradient of glass transition temperature in filled elastomers. *Europhys. Lett.* **2003**, *64*, 50–56.

(17) Mujtaba, A.; Keller, M.; Ilisch, S.; Radusch, H.; Thurn-Albrecht, T.; Saalwachter, K.; Beiner, M. Mechanical Properties and Cross-Link Density of Styrene–Butadiene Model Composites Containing Fillers with Bimodal Particle Size Distribution. *Macromolecules* **2012**, *45*, 6504–6515.

(18) Mujtaba, A.; Keller, M.; Ilisch, S.; Radusch, H.-J.; Beiner, M.; Thurn-Albrecht, T.; Saalwächter, K. Detection of Surface-Immobilized Components and Their Role in Viscoelastic Reinforcement of Rubber–Silica Nanocomposites. *ACS Macro Lett.* **2014**, *3*, 481–485.

(19) Le Gulluche, A.-C.; Pantoustier, N.; Brûlet, A.; Sanseau, O.; Sotta, P.; Marcellan, A. The role of polymer-particle adhesion in the reinforcement of hybrid hydrogels. *Macromolecules* **2023**,

(20) Petit, L. Responsive hybrid self-assemblies in aqueous media. *Langmuir* **2007**, *23*, 147–158.

(21) Perrin, E.; Schoen, M.; Coudert, F. X.; Boutin, A. Structure and Dynamics of Solvated Polymers near a Silica Surface: On the Different Roles Played by Solvent. *J. Phys. Chem. B* **2018**, *122*, 4573–4582.

(22) Laurens, J.; Jolly, J.; Ovarlez, G.; Fay, H.; Chaussée, T.; Sotta, P. Competitive Adsorption between a Polymer and Solvents onto Silica. *Langmuir* **2020**, *36*, 7669–7680.

(23) Gong, J.; Osada, Y. Double-Networks Hydrogels with Extremely High Strength. *Advanced Materials* **2003**, *15*, 1155–1158.

(24) Nakajima, T.; Furukawa, H.; Tanaka, Y.; Kurokawa, T.; Osada, Y.; Gong, J. P. True Chemical Structure of Double Network Hydrogels. *Macromolecules* **2009**, *42*, 2184–2189.

(25) Gong, J. P. Why are double network hydrogels so tough? *Soft Matter* **2010**, *6*, 2583–2590.

(26) Nakajima, T.; Fukuda, Y.; Kurokawa, T.; Sakai, T.; Chung, J. P., U. i. andGong True Chemical Structure of Double Network Hydrogels. *ACS Macro Letters* **2013**, *2*, 518.

(27) Okomura, Y.; Ito, K. The Polyrotaxane Gel: A Topological Gel by Figure-of-Eight Cross-links. *Advanced Materials* **2001**, *13*, 485–487.

(28) Harwood, J. A. C.; Mullins, L.; Payne, A. R. Strees Softening in Natural Rubber Vulcanizates. Part 2. Stress Softening Effects in Pure Gum and Filler Loaded Rubbers. *Journal of Applied Polymer Science* **1965**, *9*, 3011–3021.

(29) Nielsen, L. E.; Landel, R. F. *Mechanical Properties of Polymers and Composites*; Marcel Dekker: New York, 1994.

(30) Huber, G.; Vilgis, T. A.; Heinrich, G. Universal properties in the dynamical deformation of filled rubbers. *J. Phys.-Condens. Mat.* **1996**, *8*, L409.

(31) Papon, A.; Saalwachter, K.; Guy, K.; Lequeux, F.; Montes, H. Low Field NMR Investigations of Nanocomposites: Polymer Dynamics and Network Effects. *Macromolecules* **2011**, *44*, 913–922.

(32) Hyun, K.; Nam, J. G.; Wilhelm, M.; H., A. K.; ; J., L. S. Nonlinear response of complex fluids under LAOS (large amplitude oscillatory shear) flow. *Korea-Australia Rheology Journal* **2003**, *15*, 97–105.

(33) Hess, A.; Aksel, N. Yielding and structural relaxation in soft materials: evaluation of strain-rate frequency superposition data by the stress decomposition method. *Phys Rev E Stat Nonlin Soft Matter Phys* **2011**, *84*, 051502.

(34) Huyn, K.; Whilhelm, M.; Klein, C. O.; Cho, K. S.; Nam, J. G.; Ahn, K. H.; Lee, S. J.; Ewoldt, R. H.; McKinley, G. H. A review of nonlinear oscillatory shear tests: Analysis and application of large amplitude oscillatory shear (LAOS). *Progress in Polymer Science* **2011**, *36*, 1697–1753.

(35) Papon, A.; Montes, H.; Lequeux, L., F.and Guy Nonlinear rheology of model filled elastomers. *Journal of Polymer Science Part B: Polymer Physics* **2010**, *48*, 2490–2496.

(36) Sun, W. X.; Huang, L. Z.; Yang, Y. R.; Liu, X. X.; Tong, Z. Large amplitude oscillatory shear studies on the strain-stiffening behavior of gelatin gels. *Chin. J. Polym. Sci.* **2015**, *33*, 70–83.

(37) John, J.; Ray, D.; Aswal, V. K.; Deshpande, A. P.; Varughese, S. Dissipation and strain-stiffening behavior of pectin–Ca gels under LAOS. *Soft Matter* **2019**, *15*, 6852–6866.

(38) Jung, H.; Oyinloye, T. M.; Yoon, W. B. Evaluating the mechanical response of agarose-

xanthan mixture gels using tensile testing, numarical simulation, and a large amplitude oscillatory shear (LAOS) approach. *Foods* **2022**, *11*, 4042.

(39) Goudoulas, T. B.; Didonaki, A.; Pan, S.; Fattahi, E.; Becker, T. Comparative Large Amplitude Oscillatory Shear (LAOS) Study of Ionically and Physically Crosslinked Hydrogels. *Polymers* **2023**, *15*, 1558–1570.

(40) Papon, A.; Merabia, S.; Guy, L.; Lequeux, F.; Sotta, P.; Long, D. R. Unique Nonlinear Behavior of Nano-Filled Elastomers: From the Onset of Strain Softening to Large Amplitude Shear Deformations. *Macromolecules* **2012**, *45*, 2891–2904.

(41) Orakdogen, N.; Kizilay, M.; Okay, O. Suppression of inhomogeneities in hydrogels formed by free-radical crosslinking copolymerization. *Polymer* **2005**, *46*, 11407–11415.

(42) Sudre, G.; Hourdet, D.; Cousin, F.; Creton, C.; Tran, Y. Structure of Surfaces and Interfaces of Poly(N,N-dimethylacrylamide) Hydrogels. *Langmuir* **2012**, *28*, 12282–12287.

(43) Ferry, J. D. *Viscoelastic Properties of Polymers, 3rd Edition*; Wiley, 1980.

(44) Philippoff, W. Vibrational Measurements with Large Amplitudes. *Transactions of the Society of Rheology* **1966**, *10*, 317–334.

(45) Leblanc, J. L. Fourier Transform Rheometry on Gum Elastomers. *Journal of Applied Polymer Science* **2003**, *89*, 1101–1115.

(46) Huyn, K.; Wilhelm, M. Establishing a New Mechanical Nonlinear Coefficient Q from FT-Rheology: First Investigation of Entangled Linear and Comb Polymer Model Systems. *Macromolecules* **2009**, *42*, 411–422.

(47) Kallus, S.; Willenbacher, N.; Kirsch, S.; Distler, D.; Neidhofer, T.; Wilhelm, M.; Spiess, H. W. Characterization of polymer dispersion by Fourier transform rheology. *Rheol Acta* **2001**, *40*, 552–559.

(48) Cho, K. S.; Hyun, K.; Ahn, K. H.; Lee, S. J. A geometrical interpretation of large amplitude oscillatory shear response. *Journal of Rheology* **2005**, *49*, 747–758.

(49) Link, J.; Tauban, M.; Pieri, R.; Sanseau, O.; Sotta, P. Strain-hardening and breakdown in poly(vinylidene fluoride) gels in methyl-ethyl-ketone and heptanone. *Journal of Polymer Science* **2022**, 1–14.

(50) Kang, H.; Wen, Q.; Janmey, P. Nonlinear Elasticity of Stiff Filament Networks: Strain Stiffening, Negative Normal Stress, and Filament Alignment in Fibrin Gels. *J. Phys. Chem* **2009**, *113*, 3799–3805.

(51) Yang, Z.; Hemar, Y.; Hilliou, L.; Gilbert, E. P.; McGillivray, D. J.; Williams, M. A. K.; Chaieb, S. Nonlinear Behavior of Gelatin Networks Reveals a Hierarchical Structure. *Biomacromolecules* **2016**, *17*, 590–600.

(52) Wang, J.; Benyahia, L.; Chassenieux, C.; Tassin, J. F.; Nicolai, T. Shear-induced gelation of associative polyelectrolytes. *Polymer* **2010**, *51*, 1964–1971.

(53) Fan, Y.; Liao, H. Experimental studies on the relaxation behavior of commercial polymer melts. *Journal of Applied Polymer Science* **2008**, *110*, 1520–1530.

(54) Iler, R. K. *The Chemistry of Silica*; John Wiley and Sons: New York, 1979.

(55) Griot, O.; Kitchener, J. A. Role of Surface Silanol Groups in the Flocculation of Silica Suspensions by Polyacrylamide Part 1 .Chemistry of the Adsorption Process. *Transactions of the Faraday Society* **1965**, *61*, 1026–1031.

(56) Griot, O.; Kitchener, J. A. Role of Surface Silanol Groups in the Flocculation of Silica Suspensions by Polyacrylamide Part 2.Surface changes of silica suspensions on ageing. *Transactions of the Faraday Society* **1965**, *61*, 1032–1038.

(57) Percus, J. K.; Yevick, G. J. Analysis of Classical Statistical Mechanics by Means of Collective Coordinates. *The Physical Review* **1958**, *110*, 1–13.

(58) Menon, S. V. G.; Manohar, C.; Rao, K. S. A new interpretation of the sticky hard sphere model. *J. Chem. Phys.* **1991**, *95*, 9186–9190.

(59) Pedersen, J. S. In *Modelling of small-angle scattering data from colloids and polymer systems*; Lindner, P., Zemb, T., Eds.; North Holland, Elsevier: Amsterdam, 2002; p 391.

(60) Hollamby, M. J. Practical applications of small-angle neutron scattering. *Phys. Chem. Chem. Phys.* **2013**, *15*, 10566–10579.

(61) Kumar, S. K.; Jouault, N. Nanocomposites with Polymer Grafted Nanoparticles. *Macromolecules* **2013**, *46*, 3199–3214.

(62) Genix, A.-C.; Bocharova, V.; Carroll, B.; Lehmann, M.; Saito, T.; Krueger, S.; He, L.; Dieudonné-George, P.; Sokolov, A. P.; Oberdisse, J. Understanding the Static Interfacial Polymer Layer by Exploring the Dispersion States of Nanocomposites. *ACS Appl. Mater. Interfaces* **2019**, *11*, 17863–17872.

(63) Song, L.; Patil, S.; Song, Y.; Chen, L.; Tian, F.; Chen, L.; Li, X.; Li, L.; Cheng, S. Nanoparticle Clustering and Viscoelastic Properties of Polymer Nanocomposites with Non-Attractive Polymer-Nanoparticle Interactions. *Macromolecules* **2022**, *55*, 7626–7636.

(64) Genix, A.-C.; Bocharova, V.; Carroll, B.; Dieudonné-George, P.; Chauveau, E.; Sokolov, A. P.; Oberdisse, J. How Tuning Interfaces Impacts the Dynamics and Structure of Polymer Nanocomposites Simultaneously. *ACS Appl. Mater. Interfaces* **2023**, *15*, 7496–7510.

(65) Berriot, J.; Lequeux, F.; Montes, H.; H., P. Reinforcement of model filled elastomers: experimental and theoretical approach of swelling properties. *Polymer* **2002**, *43*, 6131–6138.

(66) Kraus, G. Swelling of filler-reinforced vulcanizates. *J. Appl. Polym. Sci.* **1963**, *7*, 861–871.

(67) Maier, P. G.; Goritz, D. Molecular interpretation of the Payne effect. *Kautschuk Gummi Kunststoffe* **1996**, *49*, 18–21.

(68) Diani, J.; Fayolle, B.; Gilormini, P. A review on the Mullins effect. *European Polymer Journal* **2009**, *45*, 601–612.

(69) Kong, H. J.; Wong, E.; Mooney, D. J. Independent Control of Rigidity and Toughness of Polymeric Hydrogels. *Macromolecules* **2003**, *36*, 4585–4588.

(70) Ng, T. S. K.; McKinley, G. H. Power law gels at finite strains: The nonlinear rheology of gluten gels. *Journal of Rheology* **2008**, *52*, 417–449.

(71) Ng, T. S. K.; McKinley, G. H. Large amplitude oscillatory shear flow of gluten dough: A model power-law gel. *Journal of Rheology* **2011**, *55*, 627–654.

(72) Hao, J.; Weiss, R. A. Viscoelastic and Mechanical Behavior of Hydrophobically Modified Hydrogels. *Macromolecules* **2011**, *44*, 9390–9398.

(73) Chippada, U.; Yurke, B.; Langrana, N. Simultaneous determination of Young's modulus, shear modulus, and Poisson's ratio of soft hydrogels. *Journal of Materials Research* **2011**, *25*, 545–555.

(74) Perez-Aparicio, R.; Vieyres, A.; Albouy, P. A.; Sanseau, O.; Vanel, L.; Long, D. R.; Sotta, P. Reinforcement in Natural Rubber Elastomer Nanocomposites: Breakdown of Entropic Elasticity. *Macromolecules* **2013**, *46*, 8964–8972.

(75) Berriot, J.; Montes, H.; Lequeux, F.; , D., Long; Sotta, P. Evidence for the Shift of the Glass Transition near the Particles in Silica-Filled Elastomers. *Macromolecules* **2002**, *35*, 9756–9762.

(76) Klüppel, M.; Schuster, R. H. Structure and Properties of Reinforcing Fractal Filler Networks in Elastomers. *Rubber Chemistry and Technology* **2008**, *70*, 243–255.

(77) Merabia, S.; Sotta, P.; Long, D. R. A Microscopic Model for the Reinforcement and the Nonlinear Behavior of Filled Elastomers and Thermoplastic Elastomers (Payne and Mullins Effects). *Macromolecules* **2008**, *41*, 8252–8266.

(78) Merabia, S.; Sotta, P.; Long, D. R. Unique Plastic and Recovery Behavior of Nanofilled Elastomers and Thermoplastic Elastomers (Payne and Mullins Effects). *Journal of Polymer Science: Part B: Polymer Physics* **2010**, *48*, 1495–1508.

(79) Joshi, Y. M.; Petekidis, G. Yield stress fluids and ageing. *Rheologica Acta* **2018**, *57*, 521–549.

(80) Moghimi, E.; Schofield, A. B.; Petekidis, G. Yielding and resolidification of colloidal gels under constant stress. *J. Phys.: Condens. Matter* **2021**, *33*, 284002.

(81) Rajaram, B.; Mohraz, A. Microstructural response of dilute colloidal gels to nonlinear shear deformation. *Soft Matter* **2010**, *6*, 2246–2259.